

UNCONDITIONAL BOUND-PRESERVING AND ENERGY-DISSIPATING FINITE-VOLUME SCHEMES FOR THE CAHN-HILLIARD EQUATION

RAFAEL BAILO, JOSÉ A. CARRILLO, SERAFIM KALLIADASIS, AND SERGIO P. PEREZ

ABSTRACT. We propose finite-volume schemes for the Cahn-Hilliard equation that unconditionally and discretely satisfy the boundedness of the phase field and the free-energy dissipation. Our numerical framework is applicable to a variety of free-energy potentials including the Ginzburg-Landau and Flory-Huggins, general wetting boundary conditions and degenerate mobilities. Its central thrust is the finite-volume upwind methodology, which we combine with a semi-implicit formulation based on the classical convex-splitting approach for the free-energy terms. Extension to an arbitrary number of dimensions is straightforward thanks to their cost-saving dimensional-splitting nature, which allows to efficiently solve higher-dimensional simulations with a simple parallelization. The numerical schemes are validated and tested in a variety of prototypical configurations with different numbers of dimensions and a rich variety of contact angles between droplets and substrates.

1. INTRODUCTION

The Cahn-Hilliard (CH) equation is a popular phase-field model initially proposed by Cahn and Hilliard [16] to describe the process of phase separation in binary alloys. Since then it has found applicability in a wide variety of modelling problems, from capillarity and wetting phenomena [3, 53], diblock copolymer molecules [62] and tumor growth [34, 58] to image inpainting [10, 13, 19], topology optimization [63] and many more [41]. Similar to other phase-field models, the CH equation avoids the explicit treatment of sharp interfaces altogether by replacing them with thin transition regions through which pertinent variables and physical properties vary rapidly but continuously. The CH equation has a gradient-flow structure of the form

$$(1) \quad \frac{\partial \phi}{\partial t} = \nabla \cdot \left(M(\phi) \nabla \frac{\delta \mathcal{F}[\phi]}{\delta \phi} \right),$$

where ϕ is the phase-field, which plays the role of an order parameter and describes the phases of the system and is a continuous function depending on time t and space x . In a binary system it takes on the limiting values $\phi = 1$ in one phase and $\phi = -1$ in the other phase.

The free energy of the system $\mathcal{F}[\phi]$ satisfies

$$(2) \quad \mathcal{F}[\phi] = \int_{\Omega} \left(H(\phi) + \frac{\epsilon^2}{2} |\nabla \phi|^2 \right) d\Omega + \int_{\partial\Omega} f_w(\phi, \beta) ds,$$

where $H(\phi)$ is a double-well potential with minima corresponding to the stable phases in the system, ϵ is a positive parameter related to the diffuse-interface width (e.g. [21]) and $f_w(\phi, \beta)$ is the wall free energy which depends on the phase field at the wall and the (equilibrium) contact angle β (e.g. [59]) – see Fig. 1 for a schematic of a droplet on a solid substrate with contact angle β). From now on $f'_w(\phi, \beta)$ denotes the derivative of $f_w(\phi, \beta)$ with respect to the phase field ϕ . The variation of the free energy with respect to the phase field $\frac{\delta \mathcal{F}[\phi]}{\delta \phi}$ is typically denoted as the chemical potential ξ . The

(Rafael Bailo) UNIV. LILLE, CNRS, UMR 8524 - LABORATOIRE PAUL PAINLEVÉ, F-59000 LILLE, FRANCE
 (José A. Carrillo) MATHEMATICAL INSTITUTE, UNIVERSITY OF OXFORD, OX2 6GG OXFORD, UK
 (Serafim Kalliadasis) DEPARTMENT OF CHEMICAL ENGINEERING, IMPERIAL COLLEGE LONDON, SW7 2AZ, UK
 (Sergio P. Perez) DEPARTMENTS OF CHEMICAL ENGINEERING AND MATHEMATICS, IMPERIAL COLLEGE LONDON, SW7 2AZ, UK

E-mail addresses: rafael.bailo@univ-lille.fr, carrillo@maths.ox.ac.uk, s.kalliadasis@imperial.ac.uk, sergio.perez15@imperial.ac.uk.

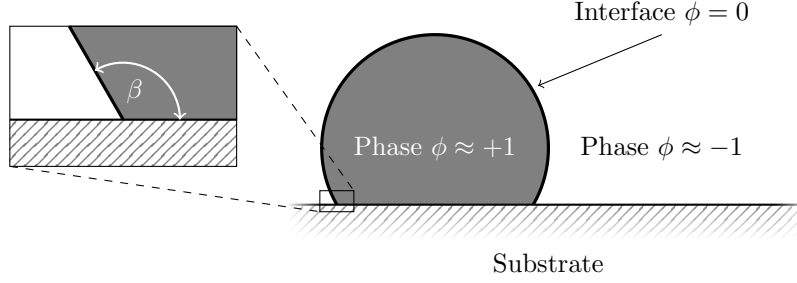


FIGURE 1. Schematic of a sessile droplet with $\phi \approx 1$ on a solid substrate and surrounded by a fluid with $\phi \approx -1$. The contact angle between the droplet and substrate is defined as β .

mobility term $M(\rho)$ is usually taken as a degenerate mobility satisfying a quadratic polynomial with roots at $\phi = \pm 1$,

$$(3) \quad M(\phi) = M_0(1 - \phi)(1 + \phi),$$

but it can be taken just as a constant, $M(\phi) = M_0$.

The boundary conditions imposed for the CH equation in (1) are a combination of the natural boundary condition for the wall free energy and no-flux for the chemical potential [3, 43],

$$(4) \quad \epsilon^2 \nabla \phi \cdot \mathbf{n} = -f'_w(\phi, \beta), \quad M(\phi) \nabla \xi \cdot \mathbf{n} = 0,$$

where \mathbf{n} is an inward-pointing unit vector normal to the wall. The form of the term $f_w(\phi)$ has received considerable attention in the literature, starting from the early contributions in the field where a linear form was stipulated, e.g. [49]. Here we assume that the function f_w has bounded second derivative on $[-1, 1]$, so that it can be split into a convex part and a concave part satisfying

$$(5) \quad f_w(\phi, \beta) = f_{c,w}(\phi, \beta) - f_{e,w}(\phi, \beta),$$

where $f_{c,w}$ and $f_{e,w}$ are convex functions. A good choice is the cubic form [3, 53–55], which is the lowest-order polynomial to allow for the minimization of the wall free energy for the bulk densities, while at the same time preventing the formation of boundary layers,

$$(6) \quad f_w(\phi, \beta) = \frac{\epsilon\sqrt{2}}{2} \cos \beta \left(\frac{\phi^3}{3} - \phi \right).$$

This cubic form alleviates the discontinuity within the realm of the diffuse-interface formulation without any additional physics. We note that the convex-concave splitting of this cubic function depends on the choice of β . Here we employ

$$f_{c,w}(\phi, \beta) = \begin{cases} \frac{\epsilon\sqrt{2}}{2} \cos \beta \left(\frac{\phi^3}{3} - \phi + \phi^2 \right) & \text{if } \cos \beta \geq 0, \\ -\frac{\epsilon\sqrt{2}}{2} \cos \beta \phi^2 & \text{otherwise,} \end{cases}$$

$$f_{e,w}(\phi, \beta) = f_{c,w}(\phi, \beta) - f_w(\phi, \beta),$$

so that $f_{c,w}(\phi, \beta)$ and $f_{e,w}(\phi, \beta)$ are convex for $\phi \in [-1, 1]$.

The variation of the free energy (2) with respect to ϕ follows from

$$\begin{aligned} \frac{d}{d\gamma} \mathcal{F}[\phi + \gamma\Psi] \Big|_{\gamma=0} &= \int_{\Omega} (\Psi H'(\phi) + \epsilon^2 \nabla \phi \cdot \nabla \Psi) d\Omega + \int_{\partial\Omega} \Psi f'_w(\phi, \beta) ds \\ &= \int_{\Omega} (H'(\phi) - \epsilon^2 \Delta \phi) \Psi d\Omega + \int_{\partial\Omega} (\epsilon^2 \nabla \phi \cdot \mathbf{n} + f'_w(\phi, \beta)) \Psi ds, \end{aligned}$$

from which one can apply the boundary conditions (4) to derive an expression for the chemical potential ξ ,

$$(7) \quad \xi = \frac{\delta \mathcal{F}[\phi]}{\delta \phi} = H'(\phi) - \epsilon^2 \Delta \phi.$$

The free energy (2) experiences a temporal decay due to the gradient-flow structure of the CH equation in (1). This is one of the main properties of gradient flows and is obtained by differentiating the free energy $\mathcal{F}[\phi]$ with respect to time and applying the boundary conditions in (4), leading to

$$\frac{d}{dt} \mathcal{F}[\phi] = - \int_{\Omega} M(\phi) \left| \nabla \frac{\delta \mathcal{F}[\phi]}{\delta \phi} \right|^2 d\Omega.$$

Mimicking this free-energy dissipation at the discrete level has been the aim of many numerical works on the CH equation. A scheme endowed with such discrete property is categorized as energy-stable, and the first unconditionally energy-stable scheme was devised by Eyre [31], who put forward the popular convex-splitting technique by which the potential $H(\phi)$ is separated in implicit contractive (convex) and explicit expansive (concave) terms. In fact this semi-implicit formulation has proven so far to be the only method of deriving unconditional energy-stable schemes, and one can show that fully implicit schemes for nonlinear systems such as the CH equation are only conditionally energy-stable depending on the time-step. This counter-intuitive fact has been recently analyzed in [61], where the authors prove that the convex-splitting scheme for the CH model is exactly the same as the fully-implicit for a different model that is a nontrivial perturbation of the original CH, and the gain of stability is at the expense of a possible loss of accuracy. In any case, the convex-splitting technique is a mainstream ingredient in the construction of energy-stable schemes for the CH equation, and has been successfully applied in various discretization strategies such as finite differences [33, 36], finite volumes [27], finite elements [7, 9, 28, 58], spectral methods [38] and discontinuous Galerkin schemes [2] (see [57] for an extensive review of energy-stable schemes for the CH equation). A recent and promising strategy to design energy-stable schemes is the so-called scalar auxiliary variable [50, 51].

The convex-splitting technique has been applied for different choices of the potential $H(\phi)$. The two main ones in the literature [8, 57] that we apply in this work are: the Ginzburg-Landau double-well potential,

$$(8) \quad H(\phi) = \frac{1}{4} (\phi^2 - 1)^2;$$

and the logarithmic potential $H_{log}(\phi)$,

$$(9) \quad H_{log}(\phi) = \frac{\theta}{2} \left[(1 + \phi) \ln \left(\frac{1 + \phi}{2} \right) + (1 - \phi) \ln \left(\frac{1 - \phi}{2} \right) \right] + \frac{\theta_c}{2} (1 - \phi^2) \text{ for } \phi \in (-1, 1),$$

where θ and θ_c are positive constants with $\theta < \theta_c$, corresponding to the absolute temperature and absolute critical temperature, respectively. The logarithmic potential, usually referred to as the Flory-Huggins energy potential in the polymer-science community [29], is considered more physically realistic in comparison to the polynomial double-well potential in (8) because it can be mathematically derived from regular or ideal solution theories [29, 42]. It is, however, singular as ϕ approaches -1 or 1 , in contrast to the double-well potential (8). The usual convex-splitting for the double-well (8) and logarithmic (9) potentials satisfy

$$H(\phi) = H_c(\phi) - H_e(\phi) = \frac{\phi^4 + 1}{4} - \frac{\phi^2}{2},$$

$$H_{log}(\phi) = H_{c,log}(\phi) - H_{e,log}(\phi) = \frac{\theta}{2} \left[(1 + \phi) \ln \left(\frac{1 + \phi}{2} \right) + (1 - \phi) \ln \left(\frac{1 - \phi}{2} \right) \right] - \left(-\frac{\theta_c}{2} (1 - \phi^2) \right),$$

so that all the functions H_c , H_e , $H_{c,log}$, and $H_{e,log}$ are convex.

Another fundamental property that has received much attention, both in terms of PDE analysis and construction of numerical schemes, is the maximum principle or boundedness of the phase-field. On the one hand, the phase-field solution of the CH equation with logarithmic potential satisfies $|\phi| < 1$ due

to the singularities of the potential (9) at $\phi = \pm 1$, both for degenerate and constant mobilities. This has already been proved at the PDE level in various works [1, 44], including for degenerate mobilities of the type (3) in [8, 30]. On the other hand, for the double-well potential (8) the phase-field solution might leave the interval $(-1, 1)$ in the general case [24, 57], due to the absence of singularities in the potential. There are, however, two cases when one can analytically prove a maximum principle for the double-well potential (8): firstly, for degenerate mobilities of the type (3) vanishing when $\phi = \pm 1$, the phase field is bounded in $|\phi| \leq 1$, as shown in [30]; secondly, for general mobilities by truncating the potential (8) with quadratic growth at infinities, as shown in [14] and applied in [25, 52].

The construction of numerical schemes with the discrete maximum principle property has attracted considerable attention, especially in recent years. The pioneering work by Copetti and Elliot [26] proposed a fully implicit scheme that satisfies a discrete maximum principle under a condition for Δt , which depends on ϵ and the critical temperature θ_0 . More recent works have sought to derive schemes that unconditionally satisfy the discrete maximum principle. An important contribution has been by Chen *et al.* [23], where a finite-difference scheme with unconditional discrete maximum principle for the logarithmic potential case is constructed for both constant and degenerate mobilities. In another recent work [32], the authors propose a flux-limiting technique based on high-order discontinuous Galerkin schemes and which unconditionally preserves global bounds for a family of PDEs including the CH equation. Many other works apply the truncation of the potential (8) with quadratic growth at infinities, with the objective of forcing their simulations to satisfy the discrete maximum principle when no rigorous proof can be derived [22, 52]. In spite of these remarkable efforts, there is still no scheme flexible enough to satisfy the discrete maximum principle for a general family of free energy potentials including the double-well (8) or the logarithmic (9), and at the same time allowing for wetting boundary conditions such as (4).

The main thrust of this work is precisely the construction of a finite-volume scheme that unconditionally satisfies both the discrete maximum principle and free-energy dissipation. The scheme maintains these two fundamental properties for general potentials including the double-well (8) and logarithmic (9), wetting conditions such as (5) as well as more general wall free energies, and degenerate mobilities of the type (3) vanishing when $\phi = \pm 1$. In contrast to previous works, the scheme is not restricted to only particular choices of the free energy potential such as the logarithmic one (9). In addition, for the case of the double-well potential (8) we do not rely on truncated potentials. Furthermore, the scheme is efficiently extended to higher-dimensional configurations due its flexible and cost-saving dimensional-splitting nature thanks to an upwind and finite-volume formulation. The computational cost can be further reduced with a straightforward parallelization resulting from the dimensional-splitting approach. The satisfaction of these unconditional properties imposes a trade-off in the order of our scheme, which in this work is limited to first-order accuracy. Nevertheless, the extension of this scheme to high order will be explored in future works. The present study builds naturally from our previous works aimed at designing structure-preserving finite-volume schemes for gradient flows and hydrodynamic systems, where a general free energy containing nonlocal interaction potentials drives the temporal evolution towards a steady state dictated by the minimizer of such free energy [5, 6, 17, 18, 20, 48].

In Section 2 we outline the construction of the one-dimensional (1D) semi-implicit scheme, with its properties of conservation of mass, boundedness of the phase field and free-energy dissipation – proved in Subsection 2.1. In Section 3 we continue with the 2D semi-implicit scheme based on the dimensional-splitting formulation, and its associated properties are proved in Subsection 3.1. Next, in Section 4 we present a battery of simulations for relevant applications of the CH equation. Validation of the first-order spatial convergence of our scheme, for both 1D and 2D test cases, is done in Subsection 4.1. In Subsection 4.2 we provide 1D simulations to scrutinise the effect of different free-energy potentials and mobility functions. Finally, in Subsection 4.3 we depict 2D simulations considering the evolution of an initial random field with different mobilities and including wall free-energy terms.

2. ONE-DIMENSIONAL SEMI-IMPLICIT SCHEME

For 1D finite-volume approximation of the CH equation (1) the computational domain $[0, L]$ is divided into N cells $C_i = [x_{i-1/2}, x_{i+1/2}]$, all with uniform size $\Delta x = L/N$, so that the centres of the cells satisfy $x_i = (i-1)\Delta x + \Delta x/2$, $i \in 1, \dots, N$. In each of the cells C_i we define the cell average ϕ_i as

$$\phi_i(t) = \frac{1}{\Delta x} \int_{C_i} \phi(x, t) dx.$$

Subsequently, one has to integrate the CH equation (1) over each of the cells C_i , resulting in

$$(10) \quad \phi_i^{n+1} - \phi_i^n = -\frac{\Delta t}{\Delta x} \left(F_{i+1/2}^{n+1} - F_{i-1/2}^{n+1} \right).$$

For the approximation of the flux at the boundary we follow an upwind approach inspired by Refs [5,18], with the fluxes computed as

$$(11) \quad F_{i+1/2}^{n+1} = \left(u_{i+1/2}^{n+1} \right)^+ M(\phi_i^{n+1}, \phi_{i+1}^{n+1}) + \left(u_{i+1/2}^{n+1} \right)^- M(\phi_{i+1}^{n+1}, \phi_i^{n+1})$$

where the velocity $u_{i+1/2}^{n+1}$ satisfies

$$u_{i+1/2}^{n+1} = -\frac{\xi_{i+1}^{n+1} - \xi_i^{n+1}}{\Delta x}$$

and the upwind is obtained from

$$\left(u_{i+1/2}^{n+1} \right)^+ = \max(u_{i+1/2}^{n+1}, 0), \quad \left(u_{i+1/2}^{n+1} \right)^- = \min(u_{i+1/2}^{n+1}, 0).$$

The discretized mobility in (11) is approximated with implicit density values from the left of the boundary, ϕ_i^{n+1} , and values from the right, ϕ_{i+1}^{n+1} . We construct the discretized mobility as

$$(12) \quad M(x, y) = M_0(1+x)^+(1-y)^+ \quad \text{or} \quad M(x, y) = M_0,$$

depending on the choice of mobility taken in (3). The proof of the unconditional boundedness of our numerical scheme in Subsection 2.1 relies heavily on the approximated mobility (12).

The discretized variation of the free energy ξ_i^{n+1} follows a semi-implicit formulation: the contractive part of the potential, $H_c(\rho)$, is taken as implicit; the expansive part of the potential, $H_e(\rho)$, is taken as explicit; and the Laplacian is taken as an average between the explicit and the implicit second-order discretizations. More precisely, the approximation of ξ_i^{n+1} is given by

$$(13) \quad \xi_i^{n+1} = H'_c(\phi_i^{n+1}) - H'_e(\phi_i^n) - \frac{\epsilon^2}{2} [(\Delta\phi)_i^n + (\Delta\phi)_i^{n+1}] + \frac{1}{\Delta x} W_i(\phi_i^{n+1}, \phi_i^n),$$

where $(\Delta\phi)_i$ is the discrete 1D second-order approximation of the Laplacian appearing in (7), defined as

$$(\Delta\phi)_i^n = \frac{\phi_{i+1}^n - 2\phi_i^n + \phi_{i-1}^n}{\Delta x^2}, \quad (\Delta\phi)_i^{n+1} = \frac{\phi_{i+1}^{n+1} - 2\phi_i^{n+1} + \phi_{i-1}^{n+1}}{\Delta x^2},$$

and the wetting term $W(\phi_i^{n+1}, \phi_i^n)$ is only evaluated at the boundaries,

$$(14) \quad W_i(\phi_i^{n+1}, \phi_i^n) = \begin{cases} f'_{c,w}(\phi_1^{n+1}, \beta) - f'_{e,w}(\phi_1^n, \beta) & \text{if } i = 1; \\ f'_{c,w}(\phi_N^{n+1}, \beta) - f'_{e,w}(\phi_N^n, \beta) & \text{if } i = N; \\ 0 & \text{otherwise.} \end{cases}$$

The no-flux boundary conditions (4) are implemented by taking the numerical flux to vanish at the boundaries,

$$(15) \quad F_{i-1/2}^{n+1} = 0 \quad \text{if } i = 1; \quad F_{i+1/2}^{n+1} = 0 \quad \text{if } i = N;$$

and by computing the Laplacian terms $(\Delta\phi)_i^n$ and $(\Delta\phi)_i^{n+1}$ at the boundaries as

$$(16) \quad \begin{cases} (\Delta\phi)_i^n = \frac{\phi_2^n - \phi_1^n}{\Delta x^2}, & (\Delta\phi)_i^{n+1} = \frac{\phi_2^{n+1} - \phi_1^{n+1}}{\Delta x^2} & \text{if } i = 1; \\ (\Delta\phi)_i^n = \frac{-\phi_N^n + \phi_{N-1}^n}{\Delta x^2}, & (\Delta\phi)_i^{n+1} = \frac{-\phi_N^{n+1} + \phi_{N-1}^{n+1}}{\Delta x^2} & \text{if } i = N. \end{cases}$$

2.1. Properties of the scheme. The finite-volume scheme proposed in Section 2 satisfies the following properties:

- (i) conservation of mass so that $\sum_{i=1}^N \phi_i^n = \sum_{i=1}^N \phi_i^{n+1}$;
- (ii) boundedness of the phase-field ϕ for mobilities of the form $M(\phi) = M_0(1 + \phi)(1 - \phi)$, so that if $|\phi_i^n| \leq 1 \forall i$, then $|\phi_i^{n+1}| \leq 1 \forall i$;
- (iii) dissipation of the discrete free energy, defined as

$$(17) \quad \mathcal{F}_\Delta^n = \Delta x \sum_{i=1}^N (H_e(\phi_i^n) - H_c(\phi_i^n)) + \Delta x \sum_{i=1}^{N-1} \frac{\epsilon^2}{2} |(\nabla\phi)_{i+1/2}^n|^2 + f_w(\phi_1^n) + f_w(\phi_N^n),$$

where $(\nabla\phi)_{i+1/2}^n$ is the discrete 1D approximation of the gradient at the interface, satisfying the first-order form $(\nabla\phi)_{i+1/2}^n := \frac{\phi_{i+1}^n - \phi_i^n}{\Delta x}$. The discrete dissipation is

$$(18) \quad \mathcal{F}_\Delta^{n+1} - \mathcal{F}_\Delta^n \leq -\Delta t \Delta x \sum_{i=1}^{N-1} \min(M(\phi_i^{n+1}, \phi_{i+1}^{n+1}), M(\phi_{i+1}^{n+1}, \phi_i^{n+1})) \left| u_{i+1/2}^{n+1} \right|^2 \leq 0.$$

Proof. Some of the ideas in these proofs are inspired by the studies in Refs [4, 5, 11, 18].

- (i) The conservation of mass follows from summing the finite-volume scheme (10) for all cells C_i and applying the no-flux conditions (16),

$$\sum_{i=1}^N (\phi_j^{n+1} - \phi_j^n) = -\frac{\Delta t}{\Delta x} \sum_{i=1}^N (F_{i+1/2}^{n+1} - F_{i-1/2}^{n+1}) = -\frac{\Delta t}{\Delta x} (F_{N+1/2}^{n+1} - F_{1-1/2}^{n+1}) = 0.$$

- (ii) We follow the general proof in [4] to show the boundedness of our scheme via contradiction. Without loss of generality, assume first that there is a group of contiguous cells satisfying $\phi_i^{n+1} > 1$, for some values i . The cells belonging to such group are $\{\phi_j^{n+1}, \phi_{j+1}^{n+1}, \dots, \phi_k^{n+1}\}$. The proof also applies if there are more groups or if the groups have only one cell. The next step is to sum the scheme (10) over the group of cells, resulting in

$$(19) \quad \frac{\Delta x}{\Delta t} \sum_{i=j}^k (\phi_i^{n+1} - \phi_i^n) = - (F_{k+1/2}^{n+1} - F_{j-1/2}^{n+1}).$$

Since we have assumed that $\phi_i^{n+1} > 1$ for $i \in \{j, j+1, \dots, k\}$, it follows that the left-hand side of (19) is positive. As a result, the right-hand side of (19) also has to be positive,

$$(20) \quad 0 < - (F_{k+1/2}^{n+1} - F_{j-1/2}^{n+1}) = - \left(u_{k+1/2}^{n+1} \right)^+ M(\phi_k^{n+1}, \phi_{k+1}^{n+1}) - \left(u_{k+1/2}^{n+1} \right)^- M(\phi_{k+1}^{n+1}, \phi_k^{n+1}) \\ + \left(u_{j-1/2}^{n+1} \right)^+ M(\phi_{j-1}^{n+1}, \phi_j^{n+1}) + \left(u_{j-1/2}^{n+1} \right)^- M(\phi_j^{n+1}, \phi_{j-1}^{n+1}).$$

The first and fourth terms in the right-hand side of (20) are negative since the mobility function returns a nonnegative value, due to (12), $\phi_{k+1}^{n+1} \leq 1$ and $\phi_{j-1}^{n+1} \leq 1$. The second and third terms are zero since $\phi_k^{n+1} > 1$ and $\phi_j^{n+1} > 1$, according to (12). As a result, the whole of the right-hand side of (20) is negative implying a contradiction that comes from assuming $\phi_i^{n+1} > 1$ for $i \in \{j, j+1, \dots, k\}$.

Proving that $\phi_i^{n+1} > -1$ is done by following an identical strategy based on contradiction.

- (iii) To show the energy dissipation we first have to take the finite-volume scheme in (10), multiply it over ξ_i^{n+1} in (13) and sum it over all cells C_i , yielding

$$\sum_{i=1}^N (\phi_i^{n+1} - \phi_i^n) \xi_i^{n+1} = -\frac{\Delta t}{\Delta x} \sum_{i=1}^N (F_{i+1/2}^{n+1} - F_{i-1/2}^{n+1}) \xi_i^{n+1}.$$

Then, by substituting the expression for ξ_i^{n+1} in (13) and rearranging, it follows that

$$\begin{aligned} (21) \quad \sum_{i=1}^N (\phi_i^{n+1} - \phi_i^n) \frac{\epsilon^2}{2} [(\Delta\phi)_i^n + (\Delta\phi)_i^{n+1}] &= \frac{\Delta t}{\Delta x} \sum_{i=1}^N (F_{i+1/2}^{n+1} - F_{i-1/2}^{n+1}) \xi_i^{n+1} \\ &+ \sum_{i=1}^N (\phi_i^{n+1} - \phi_i^n) (H'_c(\phi_i^{n+1}) - H'_e(\phi_i^n)) \\ &+ (\phi_1^{n+1} - \phi_1^n) \frac{W_1(\phi_1^{n+1}, \phi_1^n)}{\Delta x} + (\phi_N^{n+1} - \phi_N^n) \frac{W_N(\phi_N^{n+1}, \phi_N^n)}{\Delta x}. \end{aligned}$$

Now we proceed to subtract the discrete free energies in (17) at subsequent times,

$$\begin{aligned} (22) \quad \frac{\mathcal{F}_\Delta^{n+1} - \mathcal{F}_\Delta^n}{\Delta x} &= \sum_{i=1}^N (H_c(\phi_i^{n+1}) - H_c(\phi_i^n)) - \sum_{i=1}^N (H_e(\phi_i^{n+1}) - H_e(\phi_i^n)) \\ &+ \frac{\epsilon^2}{2} \sum_{i=1}^{N-1} (|(\nabla\phi)_{i+1/2}^{n+1}|^2 - |(\nabla\phi)_{i+1/2}^n|^2) \\ &+ \frac{1}{\Delta x} (f_w(\phi_1^{n+1}) - f_w(\phi_1^n) + f_w(\phi_N^{n+1}) - f_w(\phi_N^n)). \end{aligned}$$

The next step is to expand the term with the discrete gradients at the interfaces. For that we apply summation by parts and the boundary conditions in (16), leading to

$$\begin{aligned} (23) \quad &\frac{\epsilon^2}{2} \sum_{i=1}^{N-1} (|(\nabla\phi)_{i+1/2}^{n+1}|^2 - |(\nabla\phi)_{i+1/2}^n|^2) \\ &= \frac{\epsilon^2}{2} \sum_{i=1}^{N-1} ((\nabla\phi)_{i+1/2}^{n+1} + (\nabla\phi)_{i+1/2}^n) ((\nabla\phi)_{i+1/2}^{n+1} - (\nabla\phi)_{i+1/2}^n) \\ &= \frac{\epsilon^2}{2} \sum_{i=1}^{N-1} \left(\frac{\phi_{i+1}^{n+1} - \phi_i^{n+1}}{\Delta x} + \frac{\phi_{i+1}^n - \phi_i^n}{\Delta x} \right) \left(\frac{\phi_{i+1}^{n+1} - \phi_i^{n+1}}{\Delta x} - \frac{\phi_{i+1}^n - \phi_i^n}{\Delta x} \right) \\ &= -\frac{\epsilon^2}{2} \sum_{i=2}^{N-1} \left(\frac{\frac{\phi_{i+1}^{n+1} - \phi_i^{n+1}}{\Delta x} - \frac{\phi_i^{n+1} - \phi_{i-1}^{n+1}}{\Delta x}}{\Delta x} + \frac{\frac{\phi_{i+1}^n - \phi_i^n}{\Delta x} - \frac{\phi_i^n - \phi_{i-1}^n}{\Delta x}}{\Delta x} \right) (\phi_i^{n+1} - \phi_i^n) \\ &+ \frac{\epsilon^2}{2} \left(\frac{\phi_N^{n+1} - \phi_{N-1}^{n+1}}{\Delta x^2} + \frac{\phi_N^n - \phi_{N-1}^n}{\Delta x^2} \right) (\phi_N^{n+1} - \phi_N^n) \\ &- \frac{\epsilon^2}{2} \left(\frac{\phi_2^{n+1} - \phi_1^{n+1}}{\Delta x^2} + \frac{\phi_2^n - \phi_1^n}{\Delta x^2} \right) (\phi_1^{n+1} - \phi_1^n) \\ &= -\sum_{i=1}^N (\phi_i^{n+1} - \phi_i^n) \frac{\epsilon^2}{2} [(\Delta\phi)_i^n + (\Delta\phi)_i^{n+1}]. \end{aligned}$$

The outcome of the last computations is the left-hand side of (21). We can then connect (23) and (21) to obtain

(24)

$$\begin{aligned}
\frac{\epsilon^2}{2} \sum_{i=1}^{N-1} (|(\nabla \phi)_i^{n+1}|^2 - |(\nabla \phi)_i^n|^2) &= -\frac{\Delta t}{\Delta x} \sum_{i=1}^N (F_{i+1/2}^{n+1} - F_{i-1/2}^{n+1}) \xi_i^{n+1} \\
&\quad - \sum_{i=1}^N (\phi_i^{n+1} - \phi_i^n) (H'_c(\phi_i^{n+1}) - H'_e(\phi_i^n)) \\
&\quad - (\phi_1^{n+1} - \phi_1^n) \frac{W_1(\phi_1^{n+1}, \phi_1^n)}{\Delta x} - (\phi_N^{n+1} - \phi_N^n) \frac{W_N(\phi_N^{n+1}, \phi_N^n)}{\Delta x}.
\end{aligned}$$

Then, by taking into account (24), (22) can be rewritten as

$$\begin{aligned}
\frac{\mathcal{F}_\Delta^{n+1} - \mathcal{F}_\Delta^n}{\Delta x} &= \sum_{i=1}^N (H_c(\phi_i^{n+1}) - H_c(\phi_i^n) - (\phi_i^{n+1} - \phi_i^n) H'_c(\phi_i^{n+1})) \\
&\quad - \sum_{i=1}^N (H_e(\phi_i^{n+1}) - H_e(\phi_i^n) - (\phi_i^{n+1} - \phi_i^n) H'_e(\phi_i^n)) \\
&\quad + \frac{1}{\Delta x} (f_w(\phi_1^{n+1}) - f_w(\phi_1^n) - (\phi_1^{n+1} - \phi_1^n) W_1(\phi_1^{n+1}, \phi_1^n)) \\
&\quad + \frac{1}{\Delta x} (f_w(\phi_N^{n+1}) - f_w(\phi_N^n) - (\phi_N^{n+1} - \phi_N^n) W_N(\phi_N^{n+1}, \phi_N^n)) \\
&\quad - \frac{\Delta t}{\Delta x} \sum_{i=1}^N (F_{i+1/2}^{n+1} - F_{i-1/2}^{n+1}) \xi_i^{n+1} \\
&= I + II + III + IV + V.
\end{aligned}$$

Due to the convexity of both $H_c(\phi)$ and $H_e(\phi)$, which satisfy

$$\begin{aligned}
H_c(\phi_i^n) - H_c(\phi_i^{n+1}) - (\phi_i^n - \phi_i^{n+1}) H'_c(\phi_i^{n+1}) &\geq 0, \\
H_e(\phi_i^{n+1}) - H_e(\phi_i^n) - (\phi_i^{n+1} - \phi_i^n) H'_e(\phi_i^n) &\geq 0,
\end{aligned}$$

it results that $I \leq 0$ and $II \leq 0$.

Due to the convex splitting of f_w in (5), and the construction of $W_i(\phi_i^{n+1}, \phi_i^n)$ in (14), it follows that

$$\begin{aligned}
f_{c,w}(\phi_1^n) - f_{c,w}(\phi_1^{n+1}) - (\phi_1^n - \phi_1^{n+1}) f'_{c,w}(\phi_1^{n+1}, \beta) &\geq 0, \\
f_{e,w}(\phi_1^{n+1}) - f_{e,w}(\phi_1^n) - (\phi_1^{n+1} - \phi_1^n) f'_{e,w}(\phi_1^n, \beta) &\geq 0.
\end{aligned}$$

The same holds for $i = N$. As a result $III \leq 0$ and $IV \leq 0$.

For V we can apply the discrete summation by parts as well as the no-flux conditions in (15),

$$\begin{aligned}
III &= -\frac{\Delta t}{\Delta x} \sum_{i=1}^{N-1} F_{i+1/2}^{n+1} (\xi_i^{n+1} - \xi_{i+1}^{n+1}) = -\Delta t \sum_{i=1}^{N-1} F_{i+1/2}^{n+1} u_{i+1/2}^{n+1} \\
&= -\Delta t \sum_{i=1}^{N-1} \left(\left(u_{i+1/2}^{n+1} \right)^+ M(\phi_i^{n+1}, \phi_{i+1}^{n+1}) + \left(u_{i+1/2}^{n+1} \right)^- M(\phi_{i+1}^{n+1}, \phi_i^{n+1}) \right) u_{i+1/2}^{n+1} \\
&\leq -\Delta t \sum_{i=1}^{N-1} \min(M(\phi_i^{n+1}, \phi_{i+1}^{n+1}), M(\phi_{i+1}^{n+1}, \phi_i^{n+1})) \left| u_{i+1/2}^{n+1} \right|^2 \leq 0,
\end{aligned}$$

and this is precisely the decay rate for the discrete free energy written in (18).

□

3. TWO-DIMENSIONAL SEMI-IMPLICIT DIMENSIONAL-SPLITTING SCHEME

Here we construct a dimensional-splitting finite-volume scheme to solve the 2D CH equation (1). This scheme is more computationally-efficient than a full 2D scheme, and as we will demonstrate it satisfies the unconditional properties of decay of the discrete free energy and boundedness of the phase-field.

The 2D finite-volume approximation of the CH equation (1) starts by initially dividing the computational domain $[0, L] \times [0, L]$ in $N \times N$ cells $C_{i,j} := [x_{i-1/2}, x_{i+1/2}] \times [y_{j-1/2}, y_{j+1/2}]$, all with uniform size $\Delta x \Delta y$ so that $x_{i+1/2} - x_{i-1/2} = \Delta x$ and $y_{j+1/2} - y_{j-1/2} = \Delta y$. In each of the cells we define the cell average ϕ_i as

$$\phi_{i,j}(t) = \frac{1}{\Delta x \Delta y} \int_{C_{i,j}} \phi(x, y, t) dx dy.$$

For the dimensional-splitting approach we firstly update the solution along the x directions, for each index j corresponding to a fixed value of y_j where $j \in [1, N]$. Subsequently, we proceed in the same way along the y directions, for each index i corresponding to a fixed value a value of x_i where $i \in [1, N]$. The index r , where $r \in [1, N]$, denotes the index j of the fixed y_j value in every x direction of the first loop, and the updated average density for each x direction with $j = r$ is $\phi_{i,j}^{n,r}$. Similarly, the index $c \in [1, N]$ denotes the index i for every fixed value of x_j in each y direction of the second loop, and the updated density for each y direction with $i = c$ is $\phi_{i,j}^{n,c}$.

To begin with we march along each of the x direction of the domain, each of them at a fixed y_j with $j = r$. The initial conditions for the scheme are $\phi^{n,0} := \phi^n$. The scheme for each x direction satisfies:

Step 1.- for each $r = 1, \dots, N$ do:

$$(25a) \quad \phi_{i,j}^{n,r} = \begin{cases} \phi_{i,j}^{n,r-1} - \frac{\Delta t}{\Delta x} (F_{i+1/2,j}^{n,r} - F_{i-1/2,j}^{n,r}) & \text{if } j = r; \\ \phi_{i,j}^{n,r-1} & \text{otherwise;} \end{cases}$$

$$(25b) \quad F_{i+1/2,j}^{n,r} = \left(u_{i+1/2,j}^{n,r}\right)^+ M(\phi_{i,j}^r, \phi_{i+1,j}^r) + \left(u_{i+1/2,j}^{n,r}\right)^- M(\phi_{i+1,j}^r, \phi_{i,j}^r);$$

$$(25c) \quad \left(u_{i+1/2,j}^{n,r}\right)^+ = \max\{u_{i+1/2,j}^{n,r}, 0\}, \quad \left(u_{i+1/2,j}^{n,r}\right)^- = \min\{u_{i+1/2,j}^{n,r}, 0\};$$

$$(25d) \quad u_{i+1/2,j}^{n,r} = -\frac{\xi_{i+1,j}^{n,r} - \xi_{i,j}^{n,r}}{\Delta x};$$

$$(25e) \quad \begin{aligned} \xi_{i,j}^{n,r} &= H'_c(\phi_{i,j}^{n,r}) - H'_e(\phi_{i,j}^{n,r-1}) - \frac{\epsilon^2}{2} [(\Delta\phi)_{i,j}^{n,r-1} + (\Delta\phi)_{i,j}^{n,*}] \\ &\quad + \frac{1}{\Delta x} W_{i,j}^x(\phi_{i,j}^{n,r}, \phi_{i,j}^{n,r-1}) + \frac{1}{\Delta y} W_{i,j}^y(\phi_{i,j}^{n,r}, \phi_{i,j}^{n,r-1}); \end{aligned}$$

$$(25f) \quad (\Delta\phi)_{i,j}^{n,r-1} = \frac{\phi_{i+1,j}^{n,r-1} - 2\phi_{i,j}^{n,r-1} + \phi_{i-1,j}^{n,r-1}}{\Delta x^2} + \frac{\phi_{i,j+1}^{n,r-1} - 2\phi_{i,j}^{n,r-1} + \phi_{i,j-1}^{n,r-1}}{\Delta y^2};$$

$$(25g) \quad (\Delta\phi)_{i,j}^{n,*} = \frac{\phi_{i+1,j}^{n,r} - 2\phi_{i,j}^{n,r} + \phi_{i-1,j}^{n,r}}{\Delta x^2} + \frac{\phi_{i,j+1}^{n,r-1} - 2\phi_{i,j}^{n,r} + \phi_{i,j-1}^{n,r-1}}{\Delta y^2}.$$

The wetting terms $W_{i,j}^x(\phi_{i,j}^{n,r}, \phi_{i,j}^{n,r-1})$ and $W_{i,j}^y(\phi_{i,j}^{n,r}, \phi_{i,j}^{n,r-1})$ only apply at the boundaries and as in (14) satisfy,

$$(26) \quad W_{i,j}^x(\phi_{i,j}^{n,r}, \phi_{i,j}^{n,r-1}) = \begin{cases} f'_{c,w}(\phi_{1,j}^{n,r}, \beta) - f'_{e,w}(\phi_{1,j}^{n,r-1}, \beta) & \text{if } i = 1; \\ f'_{c,w}(\phi_{N,j}^{n,r}, \beta) - f'_{e,w}(\phi_{N,j}^{n,r-1}, \beta) & \text{if } i = N; \\ 0 & \text{otherwise;} \end{cases}$$

and

$$(27) \quad W_{i,j}^y(\phi_{i,j}^{n,r}, \phi_{i,j}^{n,r-1}) = \begin{cases} f'_{c,w}(\phi_{i,1}^{n,r}, \beta) - f'_{e,w}(\phi_{i,1}^{n,r-1}, \beta) & \text{if } j = 1; \\ f'_{c,w}(\phi_{i,N}^{n,r}, \beta) - f'_{e,w}(\phi_{i,N}^{n,r-1}, \beta) & \text{if } j = N; \\ 0 & \text{otherwise.} \end{cases}$$

The no-flux conditions (4) are numerically implemented by taking the numerical flux to vanish at the boundaries,

$$F_{i-\frac{1}{2},j}^{n,r} = 0 \quad \text{if } i = 1; \quad F_{i+1/2,j}^{n,r} = 0 \quad \text{if } i = N;$$

and by computing the Laplacian terms $(\Delta\phi)_{i,j}^{n,r-1}$ and $(\Delta\phi)_{i,j}^{n,\star}$ at the boundaries considering that

$$(28) \quad \begin{cases} \phi_{i,j}^{n,r-1} - \phi_{i-1,j}^{n,r-1} = 0, & \phi_{i,j}^{n,r} - \phi_{i-1,j}^{n,r} = 0 & \text{if } i = 1; \\ \phi_{i+1,j}^{n,r-1} - \phi_{i,j}^{n,r-1} = 0, & \phi_{i+1,j}^{n,r} - \phi_{i,j}^{n,r} = 0 & \text{if } i = N; \\ \phi_{i,j}^{n,r-1} - \phi_{i,j-1}^{n,r-1} = 0, & \phi_{i,j}^{n,r-1} - \phi_{i,j-1}^{n,r} = 0, & \phi_{i,j}^{n,r} - \phi_{i,j-1}^{n,r-1} = 0 & \text{if } j = 1; \\ \phi_{i,j+1}^{n,r-1} - \phi_{i,j}^{n,r-1} = 0, & \phi_{i,j+1}^{n,r-1} - \phi_{i,j}^{n,r} = 0, & \phi_{i,j+1}^{n,r} - \phi_{i,j}^{n,r-1} = 0 & \text{if } j = N. \end{cases}$$

Once the loop for the rows is completed, we define the intermediate density values as $\rho^{n+1/2} := \rho^{n,N}$. Subsequently, we continue through each of the y direction with index $c = 1, \dots, N$, each of them at a fixed x_i with $i = c$. The initial condition for this scheme is $\phi^{n,0} := \phi^{n+1/2}$:

Step 2.- for each $c = 1, \dots, N$ do:

$$(29a) \quad \phi_{i,j}^{n,c} = \begin{cases} \phi_{i,j}^{n,c-1} - \frac{\Delta t}{\Delta y} (G_{i,j+1/2}^{n,c} - G_{i,j-\frac{1}{2}}^{n,c}) & \text{if } i = c; \\ \phi_{i,j}^{n,c-1} & \text{otherwise;} \end{cases}$$

$$(29b) \quad G_{i,j+1/2}^{n,c} = \left(v_{i,j+1/2}^{n,c}\right)^+ M(\phi_{i,j}^c, \phi_{i,j+1}^c) + \left(v_{i,j+1/2}^{n,c}\right)^- M(\phi_{i,j+1}^c, \phi_{i,j}^c);$$

$$(29c) \quad \left(v_{i,j+1/2}^{n,c}\right)^+ = \max\{v_{i,j+1/2}^{n,c}, 0\}, \quad \left(v_{i,j+1/2}^{n,c}\right)^- = \min\{v_{i,j+1/2}^{n,c}, 0\};$$

$$(29d) \quad v_{i,j+1/2}^{n,c} = -\frac{\xi_{i,j+1}^{n,c} - \xi_{i,j}^{n,c}}{\Delta y};$$

$$(29e) \quad \begin{aligned} \xi_{i,j}^{n,c} = & H'_c(\phi_{i,j}^{n,c}) - H'_e(\phi_{i,j}^{n,c-1}) - \frac{\epsilon^2}{2} [(\Delta\phi)_{i,j}^{n,c-1} + (\Delta\phi)_{i,j}^{n,\diamond}] \\ & + \frac{1}{\Delta x} W_{i,j}^x(\phi_{i,j}^{n,c}, \phi_{i,j}^{n,c-1}) + \frac{1}{\Delta y} W_{i,j}^y(\phi_{i,j}^{n,c}, \phi_{i,j}^{n,c-1}); \end{aligned}$$

$$(29f) \quad (\Delta\phi)_{i,j}^{n,c-1} = \frac{\phi_{i+1,j}^{n,c-1} - 2\phi_{i,j}^{n,c-1} + \phi_{i-1,j}^{n,c-1}}{\Delta x^2} + \frac{\phi_{i,j+1}^{n,c-1} - 2\phi_{i,j}^{n,c-1} + \phi_{i,j-1}^{n,c-1}}{\Delta y^2};$$

$$(29g) \quad (\Delta\phi)_{i,j}^{n,\diamond} = \frac{\phi_{i+1,j}^{n,c-1} - 2\phi_{i,j}^{n,c} + \phi_{i-1,j}^{n,c-1}}{\Delta x^2} + \frac{\phi_{i,j+1}^{n,c} - 2\phi_{i,j}^{n,c} + \phi_{i,j-1}^{n,c}}{\Delta y^2}.$$

Here the terms $W_{i,j}^x(\phi_{i,j}^{n,c}, \phi_{i,j}^{n,c-1})$ and $W_{i,j}^y(\phi_{i,j}^{n,c}, \phi_{i,j}^{n,c-1})$ are defined as in (26) and (27). The no-flux conditions (4) are numerically implemented by taking the numerical flux to vanish at the boundaries,

$$G_{i,j-1/2}^{n,c} = 0 \quad \text{if } j = 1; \quad G_{i,j+1/2}^{n,c} = 0 \quad \text{if } j = N;$$

and by computing the Laplacian terms $(\Delta\phi)_{i,j}^{n,c-1}$ and $(\Delta\phi)_{i,j}^{n,\diamond}$ at the boundaries considering that

$$\begin{cases} \phi_{i,j}^{n,c-1} - \phi_{i-1,j}^{n,c-1} = 0, & \phi_{i,j}^{n,c-1} - \phi_{i-1,j}^{n,c} = 0, & \phi_{i,j}^{n,c} - \phi_{i-1,j}^{n,c-1} = 0 & \text{if } i = 1; \\ \phi_{i+1,j}^{n,c-1} - \phi_{i,j}^{n,c-1} = 0, & \phi_{i+1,j}^{n,c-1} - \phi_{i,j}^{n,c} = 0, & \phi_{i+1,j}^{n,c} - \phi_{i,j}^{n,c-1} = 0 & \text{if } i = N; \\ \phi_{i,j}^{n,c-1} - \phi_{i,j-1}^{n,c-1} = 0, & \phi_{i,j}^{n,c} - \phi_{i,j-1}^{n,c} = 0 & & \text{if } j = 1; \\ \phi_{i,j+1}^{n,c-1} - \phi_{i,j}^{n,c-1} = 0, & \phi_{i,j+1}^{n,c} - \phi_{i,j}^{n,c} = 0, & & \text{if } j = N. \end{cases}$$

Once the loop for the columns is completed, we define the final density values ρ^{n+1} after a discrete timestep Δt as $\rho^{n+1} := \rho^{n,N}$.

3.1. Properties of the dimensional-splitting 2D scheme. The dimensional-splitting 2D finite-volume scheme satisfies the following properties:

- (i) conservation of mass so that $\sum_{i,j=1}^N \phi_{i,j}^n = \sum_{i,j=1}^N \phi_{i,j}^{n+1}$;
- (ii) boundedness of the phase-field ϕ for mobilities of the form $M(\phi) = M_0(1 + \phi)(1 - \phi)$, so that if $|\phi_{i,j}^n| \leq 1 \forall i$, then $|\phi_{i,j}^{n+1}| \leq 1 \forall i$;
- (iii) dissipation of the discrete free energy, $\mathcal{F}_\Delta^{n+1} - \mathcal{F}_\Delta^n \leq 0$, with \mathcal{F}_Δ^n defined as

$$\begin{aligned}
 \mathcal{F}_\Delta^n = & \Delta x \Delta y \sum_{i,j=1}^N (H_c(\phi_{i,j}^n) - H_e(\phi_{i,j}^n)) \\
 (30) \quad & + \Delta x \Delta y \sum_{i=1}^{N-1} \sum_{j=1}^N \frac{\epsilon^2}{2} \left(\frac{\phi_{i+1,j}^n - \phi_{i,j}^n}{\Delta x} \right)^2 + \Delta x \Delta y \sum_{i=1}^N \sum_{j=1}^{N-1} \frac{\epsilon^2}{2} \left(\frac{\phi_{i,j+1}^n - \phi_{i,j}^n}{\Delta y} \right)^2 \\
 & + \Delta x \sum_{j=1}^N (f_w(\phi_{1,j}^n) + f_w(\phi_{N,j}^n)) + \Delta y \sum_{i=1}^N (f_w(\phi_{i,1}^n) + f_w(\phi_{i,N}^n)).
 \end{aligned}$$

Proof. (i) For the conservation of mass we need to show that the mass is conserved in every row and every column, and this can be done as in the 1D case of Subsection 2.1.
(ii) For the unconditional boundedness of the phase-field we need to show that the phase-field is bounded in every row and every column. This is accomplished by following the contradiction strategy employed for the 1D case of Subsection 2.1, which in this case has to be applied independently to every row and column.
(iii) For the decay of the discrete free energy in (30) we show that the discrete free energy decays for every row and for every column. For this we refer the reader to Lemmas A.1 and A.2 in Appendix A, where we firstly show that for every row r we have that

$$\mathcal{F}_\Delta(\rho^{n,r}) - \mathcal{F}_\Delta(\rho^{n,r-1}) \leq 0 \quad \forall r,$$

and, subsequently, for every column c we have that

$$\mathcal{F}_\Delta(\rho^{n,c}) - \mathcal{F}_\Delta(\rho^{n,c-1}) \leq 0 \quad \forall c.$$

Consequently, it follows that the global decay of the discrete free energy is satisfied. \square

Remark 3.1 (Full 2D scheme). It is possible to construct a full 2D implicit scheme that satisfies the unconditional boundedness and decay of the free energy. Supposing that the cost of inverting a $N \times N$ matrix is $\mathcal{O}(N^3)$, it follows that the full 2D scheme has a computational complexity of $\mathcal{O}(N^6)$, as we need to invert a $N^2 \times N^2$ matrix. Alternatively, the cost of the dimensional-splitting scheme would be $\mathcal{O}(2N^4)$, since we need to invert a $N \times N$ matrix in each of the $2N$ rows and columns. As a result, there is a significant reduction of computational cost by employing the dimensional-splitting approach, and such cost is reduced even further in higher dimensions.

Remark 3.2 (Parallelization of the dimensional-splitting scheme in two and higher dimensions). The dimensional-splitting scheme in Section 3 can be fully parallelized in order to save computational time. This is possible due to two important observations: first, the scheme does not take notice of the order of updating the rows-columns, as long as all of them are updated; second, one row or column only depends on the values of the directly adjacent rows or columns, respectively. As a result, a strategy to parallelize the dimensional splitting scheme consists in updating at the same time all the odd rows-columns, as they do not depend on one another. At the same time the even rows-columns are also updated.

4. NUMERICAL EXPERIMENTS

In this Section we test the applicability of our 1D and 2D schemes in a variety of configurations for the CH equation (1). But first, in Subsection 4.1 we test the spatial order of convergence of both schemes, showing that they satisfy a first-order spatial order of convergence. Subsequently, in Subsection 4.2 we present several test cases of 1D configurations. Finally, in Subsection 4.3 we focus on 2D simulations.

In all simulations the discrete free energy is computed as (17) and (30), for the 1D and 2D cases respectively. The full wetting boundary conditions are applied in Subsubsection 4.3.2, but for the rest of examples we assume $f_w(\phi, \beta) = 0$.

The code to reproduce all simulations is available in a Github repository [45]. The films of the 2D simulations are available in the figshare repository [46].

4.1. Order-of-convergence validation with explicit steady state. The selected test case was firstly proposed in [8], and it has subsequently served as a computational prototype adopted by many authors to validate their numerical schemes for the CH equation [39, 60]. The advantage of this test case is that an explicit steady state is known given particular initial conditions. Hence, once the steady state is reached, it can be readily utilized to measure the error of the numerical simulations for different mesh choices.

The original test case in [8] was formulated only for 1D simulations. Here, we appropriately extend it to two dimensions. We choose the logarithmic potential (9) in the deep quench limit with $\theta = 0$ and $\theta_c = 1$, so that $H_{log}(\phi) = (1 - \phi^2)/2$. The mobility satisfies the degenerate form in (3) and $\epsilon = 0.1$. The time step is $\Delta t = 0.0001$ for all simulations and we let the evolution run until $t = 0.1$.

For the 1D the spatial domain is $[0, 1]$, with the number of cells taken as 25, 50, 100 and 200 in successive simulations. For the 2D case the domain is $[0, 1] \times [0, 1]$ with the number of cells in each of the two axes as 10, 20, 40 and 80. When doubling the number of cells, the mesh size is halved and we can then compute the spatial order of the scheme as

$$\text{Order of the scheme} = \ln_2 \left(\frac{L^1 \text{ error}(\Delta x)}{L^1 \text{ error}(\Delta x/2)} \right),$$

with the L^1 error measured from the explicitly known steady state.

Following [8] we set the initial conditions of the simulation as

$$\phi_0(x, y) = \begin{cases} \cos\left(\frac{x-1/2}{\epsilon}\right) - 1, & \text{if } |x - \frac{1}{2}| \leq \frac{\pi\epsilon}{2}, \\ -1, & \text{otherwise,} \end{cases}$$

for both the 1D and 2D simulations. We notice that for the 1D simulation $y = 0 \forall x$, while for the 2D simulation the phase-field is symmetric with respect to $x = 0.5$ (see Fig. 3(a) for a depiction of the initial phase-field). With this choice of initial conditions the explicit steady state satisfies

$$(31) \quad \phi_{\text{steady}}(x, y) = \begin{cases} \frac{1}{\pi} \left[1 + \cos\left(\frac{x-1/2}{\epsilon}\right) \right] - 1, & \text{if } |x - \frac{1}{2}| \leq \pi\epsilon, \\ -1, & \text{otherwise.} \end{cases}$$

In Table 1 we present the L^1 errors and spatial order of convergence for both the 1D and 2D tests. Clearly for both cases the spatial order of convergence stabilizes around 1 after increasing the number of cells. In Fig. 2 we plot the temporal evolution of the 1D solution and the decay of the discrete free energy (17). For the latter we observe that the steady state is reached at $t \simeq 0.1$ as is evident from the plateau that the free energy at that time. In Fig. 3 we display the initial and steady phase-fields of the 1D test. The 2D free-energy decay is omitted due to its similarity to the 1D behavior in Fig. 2(b).

4.2. 1D simulations.

Number of cells	L^1 error	order
25	6.797E-03	-
50	7.136E-04	3.25
100	2.938E-04	1.28
200	1.205E-05	1.29

Number of cells	L^1 error	order
10×10	1.112E-02	-
20×20	6.752E-03	0.72
40×40	2.278E-03	1.57
80×80	7.736E-04	1.56

TABLE 1. Order-of-convergence test validating the first-order spatial accuracy of the 1D (left) and 2D (right) schemes. The errors are computed at $t = 0.1$ from the explicit solution (31) in Subsection 4.1

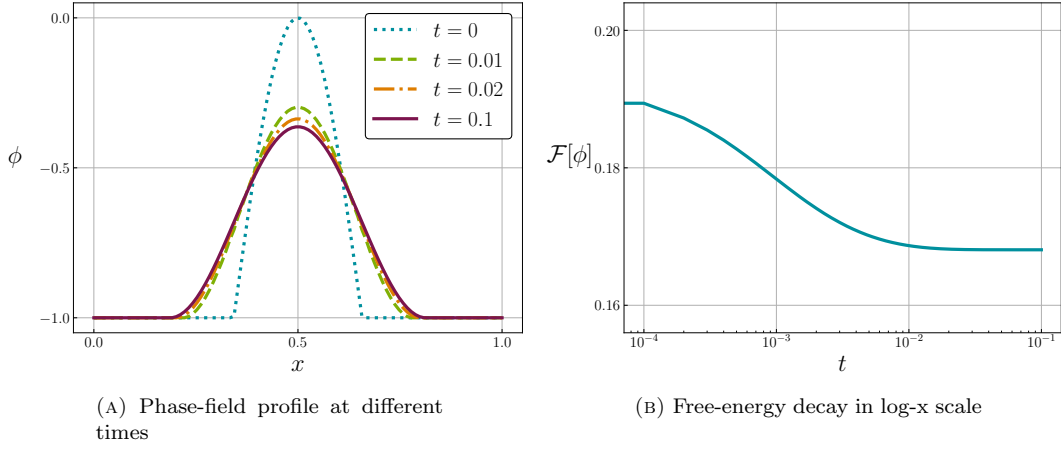


FIGURE 2. Temporal evolution for the 1D test in Subsection 4.1.

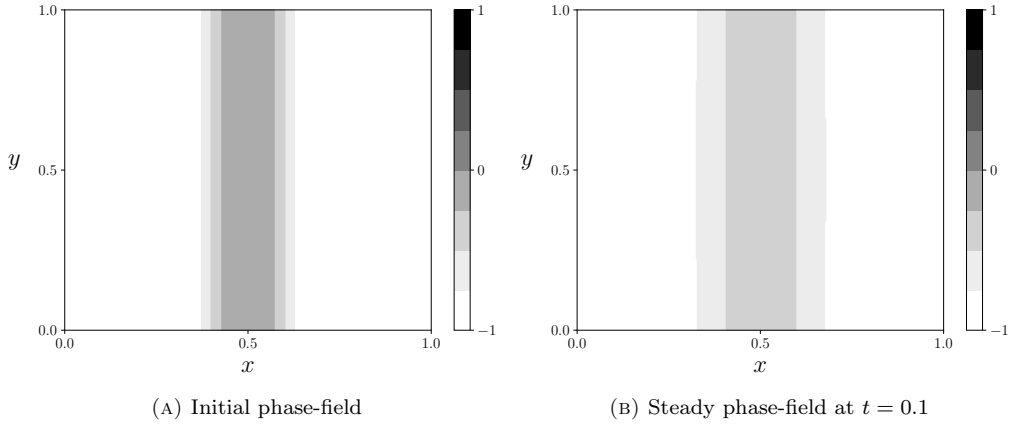


FIGURE 3. Initial and steady phase-fields for the 2D test in Subsection 4.1.

4.2.1. *Phase separation in randomized initial phase-field.* We focus on the behavior of the CH equation (1) with the double-well potential (8) and with the logarithmic potential (9). As is well known, a process of phase separation with emerging clusters at $\phi = \pm 1$ takes place during the temporal evolution, and here we explore how the choice of potential affects the temporal scales and phase-field profiles at

equilibrium. The initial phase-field is taken as $\phi_i(t=0) = r$, with r being a random variable with uniform distribution in $[-0.5, 0.5]$. After the sampling, we keep the same initial phase-field for the two simulations. The spatial domain is $x \in [-40, 40]$, and the number of cells is 200. The mobility is taken as the degenerate form in (3), and the interface parameter as $\epsilon = 1$. For the logarithmic potential we select as absolute temperature $\theta = 0.3$ and as critical temperature $\theta_c = 1$. The time step is $\Delta t = 0.01$ and we let the evolution run until $t = 30$. A similar simulation can be found in [37].

Figures 4(a) and (b) depict the temporal evolution of the phase-field, for the double-well and logarithmic potentials, respectively. There is a clear phase separation. Figures 4(c) and (d) provide a zoom of the density profile at $t = 30$, after the steady state has been reached. For the double-well potential, we observe a wider interface thickness with peaks lower than $|\phi| = 1$, while for the logarithmic potential the peaks form a plateau and have the value of $|\phi| = 1$. Lastly, in Fig. 4(e) and (f) we illustrate the evolution of the discrete free energy (17), where we observe that the logarithmic potential takes slightly less time to reach the steady state.

4.2.2. Effect of mobility with logarithmic potential. The aim here is to test the effect of choosing a constant mobility $M = 1$ versus a degenerate mobility $M = (1 - \phi)(1 + \phi)$. This example was firstly proposed in [8] and later implemented in [60]. The scheme proposed in Section 2 satisfies the boundedness of the solution only for the degenerate mobility.

As initial condition for the simulation we select

$$\phi_0(x) = \begin{cases} 1, & \text{if } 0 \leq x \leq \frac{1}{3} - \frac{1}{20} \\ 20 \left(\frac{1}{3} - x \right), & \text{if } \left| x - \frac{1}{3} \right| \leq \frac{1}{20}, \\ -20 \left| x - \frac{41}{50} \right|, & \text{if } \left| x - \frac{41}{50} \right| \leq \frac{1}{20}, \\ -1, & \text{otherwise.} \end{cases}$$

As potentials we choose the logarithmic potential (9) with $\theta = 0.3$ and $\theta_c = 1$. The spatial domain of the simulation is $x \in [0, 1]$, and the number of cells is 80. The time step is $\Delta t = 0.01$, $\epsilon = \sqrt{10^{-3}}$ and we let the evolution run until $t = 0.1$.

The results for the phase-field and free-energy evolution are displayed in Fig. 5. We notice that for the constant mobility $M = 1$ the bump at the right of the domain is quickly dissipated, while for the degenerate mobility it takes a much longer time. This happens because the bump is surrounded by a pure phase with $\phi = -1$, where the degenerate mobility cancels out. As a result, the mobility term is much higher for the constant mobility, and mass exchange occurs faster. In Fig. 5(c) and (d) we display the free energy dissipation, and the timescale to reach the steady state is clearly much shorter for the constant mobility.

4.3. 2D simulations.

4.3.1. Phase separation with different mobilities. We choose the Ginzburg-Landau double-well potential in (8). It is a widely-employed potential for benchmarking numerical schemes of the CH equation, and we refer the reader to [8, 35, 60] for similar simulations.

As initial phase-field we select $\phi_0(x, y) = -0.4 + r$, with r being a random variable with uniform distribution in $[-0.25, 0.25]$. The 2D spatial domain of the simulation is chosen as $[-0.5, 0.5] \times [-0.5, 0.5]$ with 256 cells in each of the x and y directions. The mobility is taken as the degenerate form in (3), and the interface parameter as $\epsilon = 0.18$. The time step is $\Delta t = 0.0016$ and the evolution is monitored up to $t = 1$.

The results of the two simulations, for constant and degenerate mobility, are shown in Fig. 6 for three different snapshots of time. The decay of the corresponding free energy is depicted in Fig. 7. For the case of constant mobility in Figs. 6(a), (c) and (e) we observe an initial stage of phase separation followed by a coarsening process with merging phases. From the free-energy plot in Fig. 7 we remark the short time-scale of the phase separation in comparison to the long timescale of coarsening, which in turn leads to sudden decreases of free energy when distant phases merge. The log $-x$ plot in 7(b) illustrates the exponential decay of the free energy during the short time-scale due to the initial phase

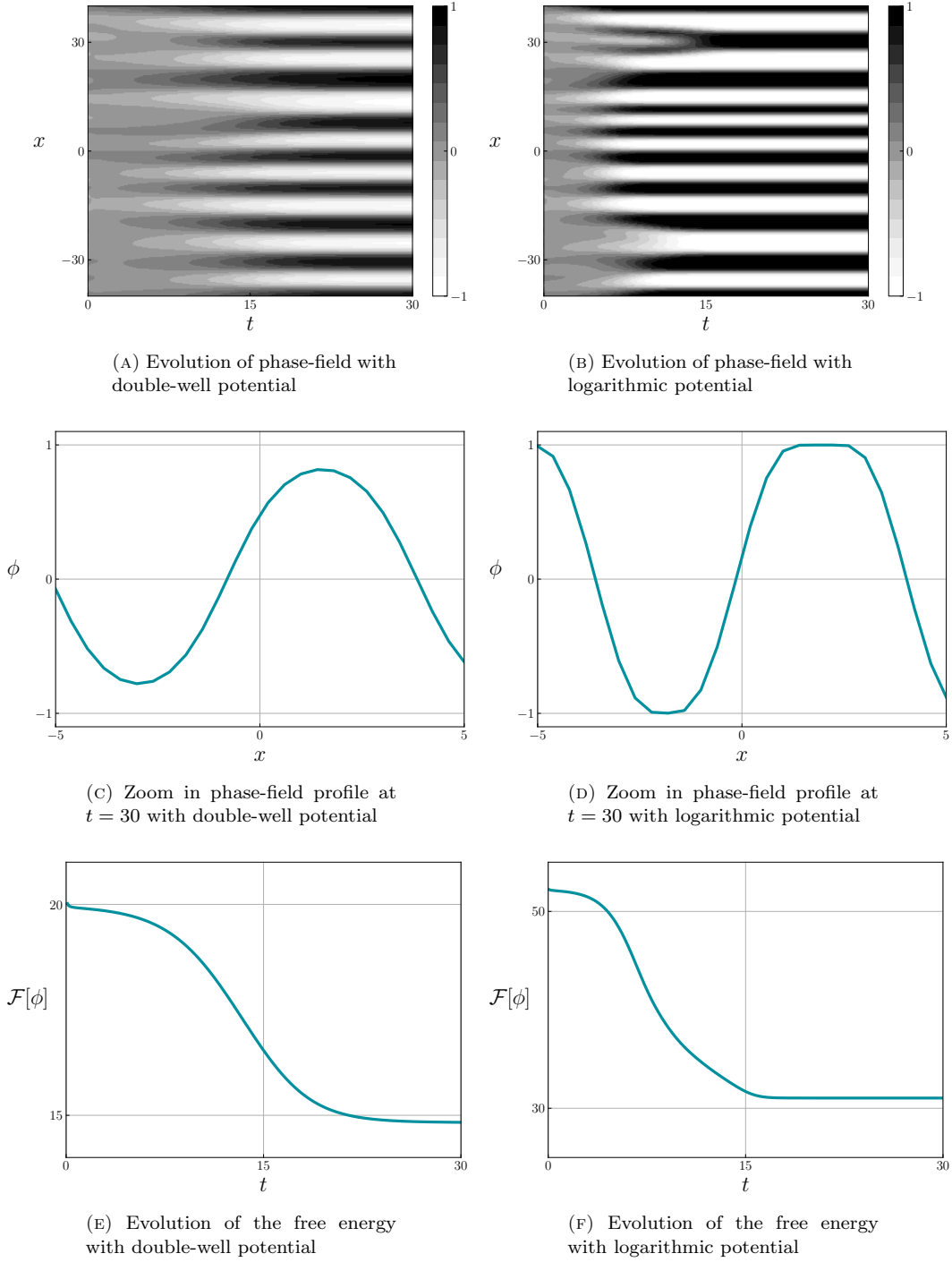


FIGURE 4. Temporal evolution for the initially-randomized phase-field in Subsection 4.2.1.

separation from a randomised field. A similar phenomenon occurs in macroscopic systems with Morse-type interaction potentials [20], where two different timescales are also present: one for the attraction

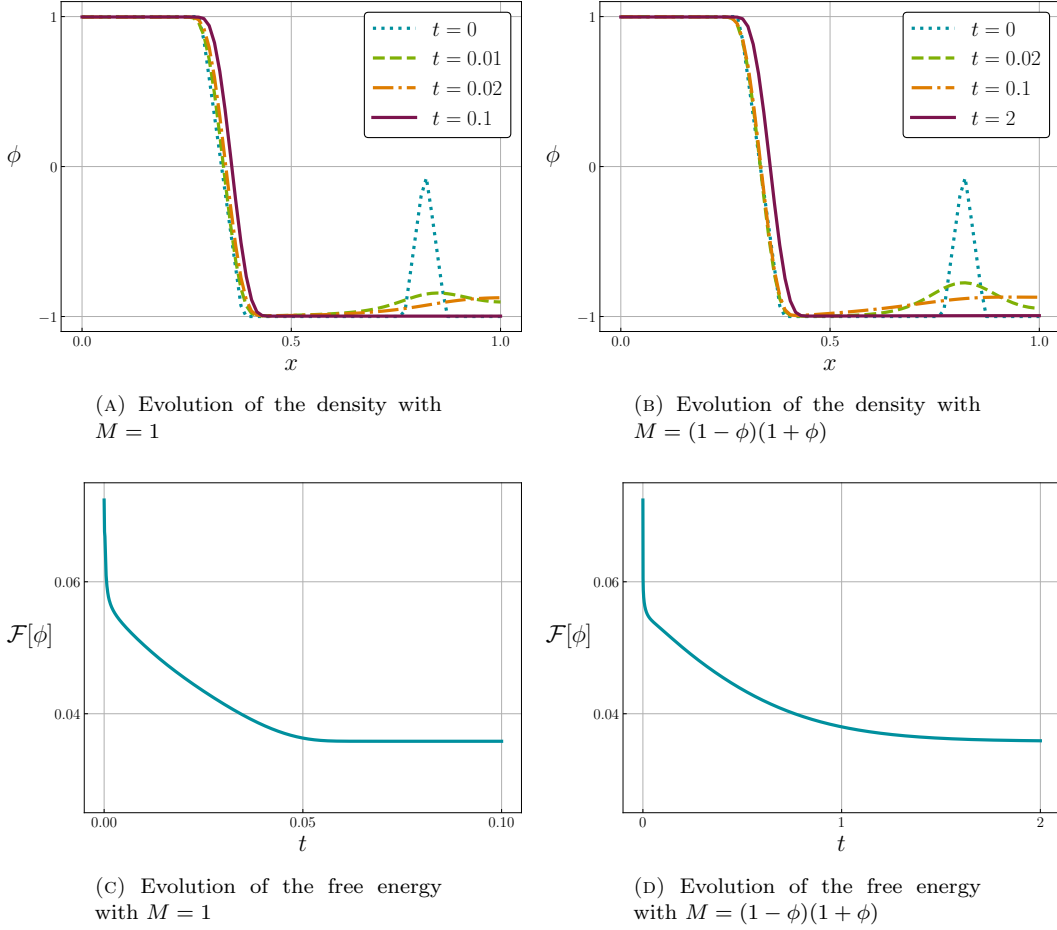


FIGURE 5. Temporal evolution for the logarithmic potential in Subsection 4.2.2.

of phases and another one for the merging process. In the final snapshot at $t = 1$ only two phases remain in the domain.

The evolution with degenerate mobility is displayed in 6(b), (d) and (f). The phase-separation stage is similar to the one with constant mobility, and as both simulations share the same initial condition, not surprisingly the first snapshots in Figs. 6(a) and (b) look alike. The initial timescales also have the same order of magnitude, as displayed in the free energy plot in Fig. 7. However, once the phases are formed there is little evolution in the system, due to the fact that the degenerate mobility is cancelled when $\phi = \pm 1$. As a consequence at $t = 1$ the phases have not yet merged, in sharp contrast to the case of constant mobility. In addition, the free energy reaches a much lower value for the case of constant mobility, a result of the merging of phases combined with reduction of interphases.

4.3.2. Contact angle in wetting phenomena. In this example we analyze wetting phenomena with sessile droplets on a flat solid substrate. In this application a fluid-fluid interface moves along the solid substrate, while a contact line is formed at the intersection between the interface and the substrate. Of special interest is the contact angle at the three-phase conjunction, which is determined by the wetting properties of the substrate.

For this setting the free energy in (2) takes into account the wetting effects at the boundary $\partial\Omega$ between the droplet and the substrate [15,43], with $f_w(\phi)$ contributing to the wall component of the free

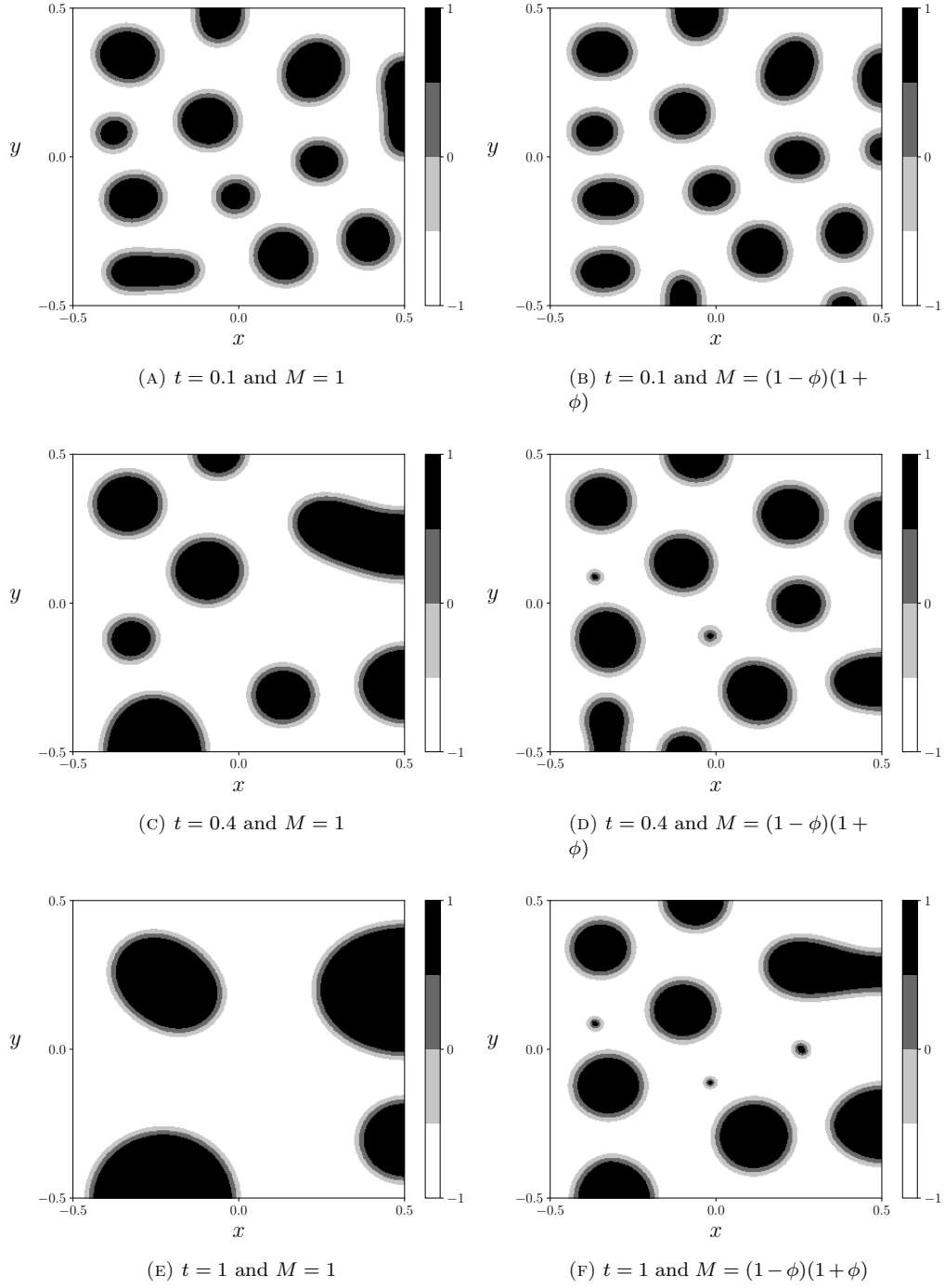


FIGURE 6. Temporal evolution for the initially randomized phase-field in Subsection 4.3.1. Comparison of constant mobility (left) versus degenerate mobility (right).

energy. The form of the term $f_w(\phi)$ has received considerable attention in the literature, starting with early works using linear forms for liquid-gas problems [49]. Here we adopt the cubic form suggested in [3, 53–55] on the basis that it is the lowest-order polynomial to allow for the minimization of the wall

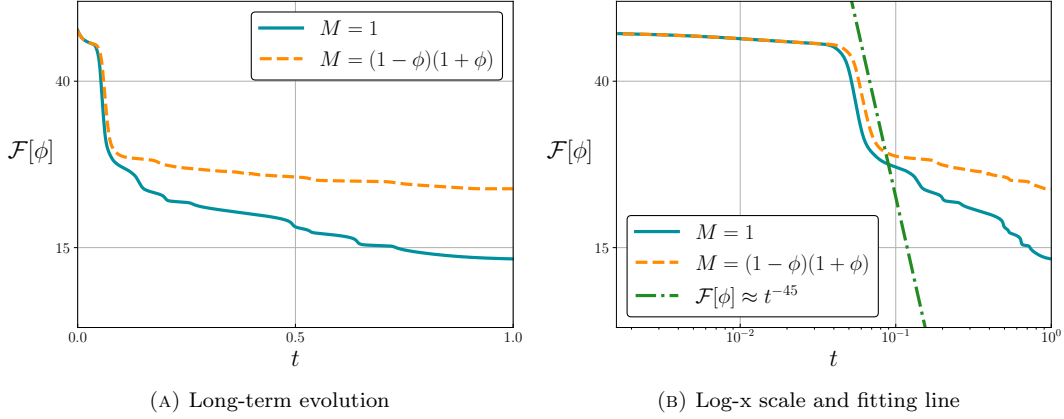


FIGURE 7. Free-energy decay in time comparing the constant-mobility and degenerate-mobility simulations in Subsection 4.3.1.

free energy for the bulk densities, while at the same time preventing the formation of boundary layers. As noted in the introduction, the basic idea is that the contact line singularity can be removed without any additional physics. Details on how exactly this works, together with the associated asymptotic analysis are given in [54, 55].

Our choice for $f_w(\phi)$ satisfies (6), where β is the equilibrium contact angle, taken here as constant. Analogous modifications of the CH model have been applied in a variety of wetting scenarios including wetting of complex topographical geometries and chemically-heterogeneous substrates, with applications from microfluidic devices [47] to polymer films [40] and rheological systems [12].

In our first simulations we check that the equilibrium contact angle of sessile droplet on flat substrate obtained with our 2D scheme in Section 3 matches with the angle β imposed in the wall free-energy term $f_w(\phi, \beta)$. This is done for five choices of β : $\pi/3$, $5\pi/12$, $\pi/2$, $7\pi/12$ and $2\pi/3$. We point out that the choice of $\beta = \pi/2$ cancels $f_w(\phi, \beta)$ since $\cos \beta$ is multiplying the rest of the terms in (6).

As initial phase in the domain $[-0.5, 0.5] \times [0, 0.4]$ we select the semicircle

$$\phi_0(x, y) = \begin{cases} 0.97 & \text{if } x^2 + y^2 < 0.25^2; \\ -0.97 & \text{if } x^2 + y^2 \geq 0.25^2. \end{cases}$$

The number of cells both in each of the x and y directions is 256. The mobility takes the degenerate form in (3), and the interface parameter is chosen as $\epsilon = 0.005$. The time step is $\Delta t = 0.001$ and we follow the evolution until $t = 0.1$. We adopt the Ginzburg-Landau double-well potential in (8). The solid substrate boundary condition is imposed along $y = 0$. It should be noted that the initial phase-field is selected with values of ± 0.97 instead of ± 1 so that the degenerate mobility is not cancelled and the simulation can proceed uninterrupted. Similar simulations but with constant mobility were performed in [3].

The equilibrium phase-fields at $t = 0.1$ are shown in Figs. 8 (a)-(e), while the free-energy dissipation comparison is depicted in 8 (f). The numerical contact angle $\hat{\beta}$ is close to the predefined angle β , and the quotient between the two is reported in the captions of Fig. 8 (a)-(e). Such numerical angle is measured by employing the Drop Shape Analysis open-source software from [56]. From Fig. 8(f) we observe that all droplets stabilize after a short time of $\simeq 0.01$. It is also clear that the angle with the largest $\cos \beta$, i.e. $\beta = \pi/3$, has the greatest free energy overall due to the contribution of $f_w(\phi, \beta)$ in (6). On the contrary, the angle $\beta = 2\pi/3$ has the lowest overall free energy. Interestingly, for the angle $\beta = \pi/2$ there is dynamical evolution even if the initial configuration already has the right contact angle. This is due to the fact that there are no interphases in the initial phase-field.

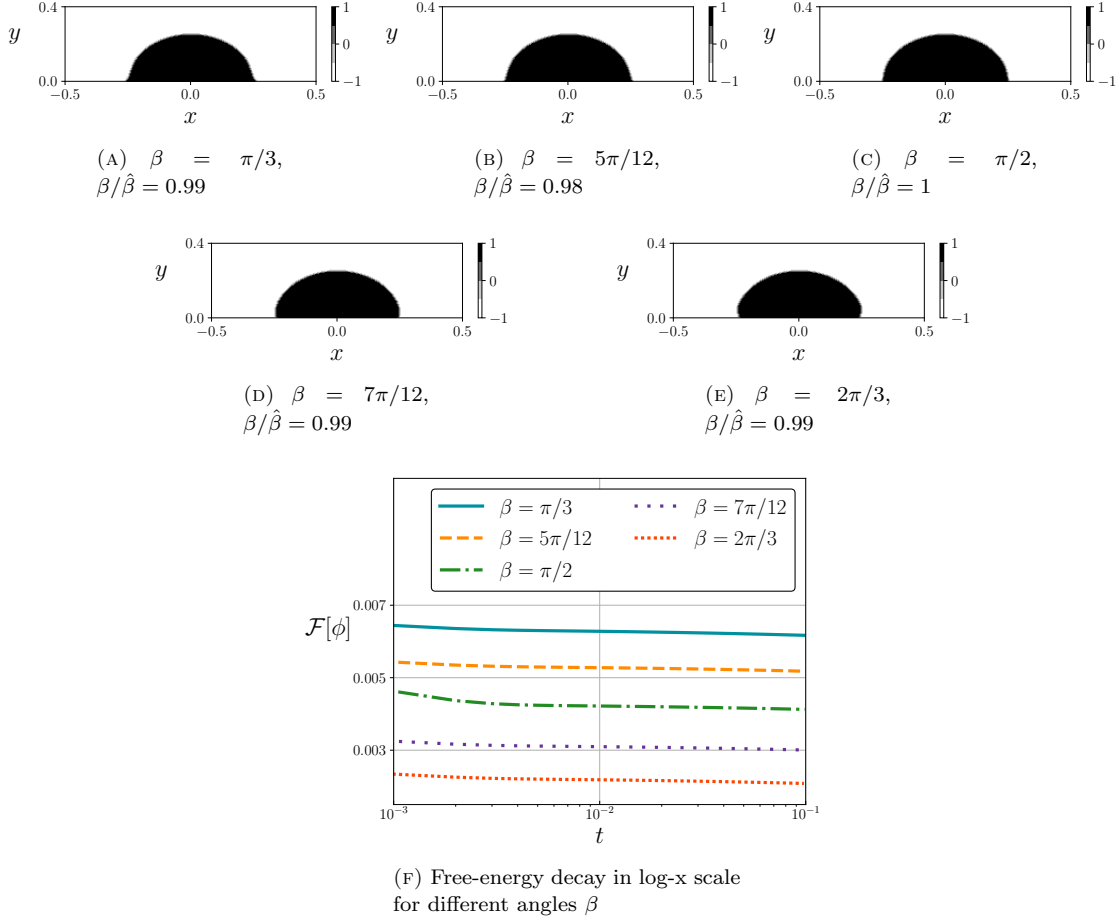


FIGURE 8. (A)-(E) Equilibrium phase-fields at $t = 2$ for different choices of angle β . (F) Dissipation of the free energy for different choices of angle β .

In the simulations that follow, we analyse the effect of contact angle on the merging of droplets on both hydrophilic ($\beta < \pi/2$) and hydrophobic ($\beta > \pi/2$) solid substrates. The objective is to show that on hydrophilic substrates droplets are prone to merging and, as a consequence, to forming a single phase; on the other hand, on hydrophobic substrates droplets tend to remain isolated.

As initial phase-field in the domain $[-1, 1] \times [0, 0.5]$ we select the two semicircles

$$\phi_0(x, y) = \begin{cases} 0.97 & \text{if } (x + 0.35)^2 + y^2 < 0.3^2 \text{ or } (x - 0.35)^2 + y^2 < 0.3^2; \\ -0.97 & \text{elsewhere.} \end{cases}$$

We now have 256 cells in the x direction and 64 in the y direction. The mobility assumes the degenerate form in (3), and the interface parameter has the value $\epsilon = 0.012$. The time step is $\Delta t = 0.0005$ and we follow the system up until $t = 15$. The employed contact angles are $\beta = \pi/4$ and $\beta = 3\pi/4$. The remaining parameters are identical to our previous simulations with single droplets.

The dynamic evolution of the droplets for the two choices of contact angle is detailed in Fig. 9(a)-(f), while the free-energy evolution can be found in 9(g). From the plots with contact angle $\beta = \pi/4$ corresponding to a hydrophilic substrate, it can be seen that the two droplets coalesce and after $t = 15$ a single phase is clearly formed. On the contrary, the droplets with contact angle $\beta = 3\pi/4$ remain distant and do not merge during the dynamic evolution. From the free-energy plots in Fig. 9(g) we

also find that the free energy reaches a plateau for both contact angles, meaning that the stationary state has been reached. We again employ a log $-x$ scale due to the significant free-energy decay at short timescales at the beginning of the simulation.

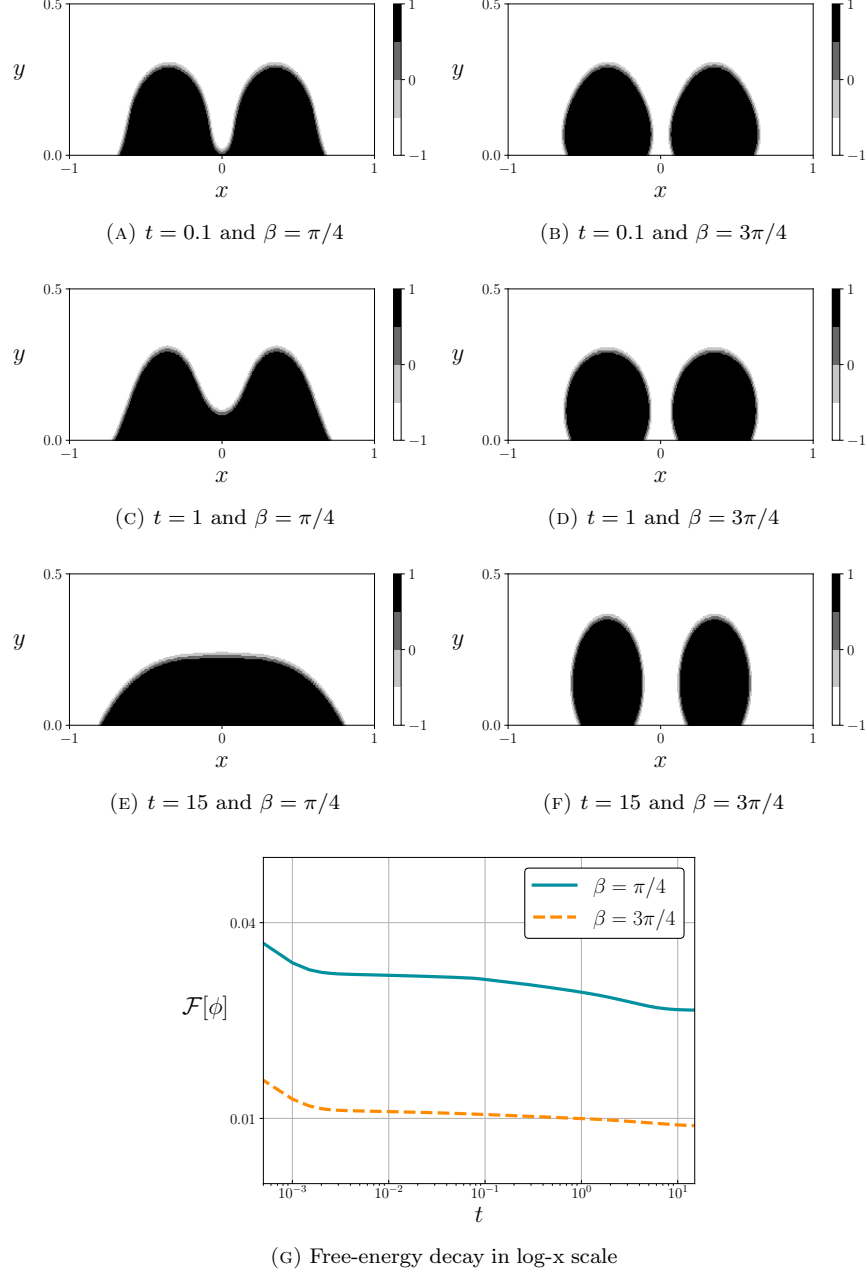


FIGURE 9. (A)-(F) Temporal evolution of two droplets with the hydrophilic angle $\beta = \pi/4$ (left) and the hydrophobic angle $\beta = 3\pi/4$ (right). (G) Comparison of free-energy decay for the two angle $\beta = \pi/4$ and $\beta = 3\pi/4$.

ACKNOWLEDGEMENTS

JAC was supported by the Advanced Grant Nonlocal-CPD (Nonlocal PDEs for Complex Particle Dynamics: Phase Transitions, Patterns and Synchronization) of the European Research Council Executive Agency (ERC) under the European Union's Horizon 2020 research and innovation programme (grant agreement No. 883363). JAC was also partially supported by the EPSRC grant number EP/T022132/1.

APPENDIX A. DISSIPATION OF THE DISCRETE FREE ENERGY IN THE DIMENSIONAL-SPLITTING SCHEME

Here we prove the dissipation of the discrete free energy in every row and every column for the dimensional-splitting 2D scheme of Subsection 3. Firstly, in Lemma A.1 we prove the dissipation of the free energy in each x -direction iteration. Subsequently, in Lemma A.2 we prove the dissipation of the free energy in each y -direction iteration. Both lemmas are necessary to show the global dissipation of the discrete free energy for the dimensional-splitting 2D scheme, as already highlighted in Subsection 3.1.

Lemma A.1. *Dissipation of the discrete free energy in each x -direction iteration. Let the discrete free energy of (2) for a particular r be defined as:*

$$\begin{aligned}
 \mathcal{F}_\Delta(\phi^{n,r}) = & \Delta x \Delta y \sum_{i,j=1}^n (H_c(\phi_{i,j}^{n,r}) - H_e(\phi_{i,j}^{n,r})) \\
 & + \Delta x \Delta y \sum_{i=1}^{N-1} \sum_{j=1}^N \frac{\epsilon^2}{2} \left(\frac{\phi_{i+1,j}^{n,r} - \phi_{i,j}^{n,r}}{\Delta x} \right)^2 + \Delta x \Delta y \sum_{i=1}^N \sum_{j=1}^{N-1} \frac{\epsilon^2}{2} \left(\frac{\phi_{i,j+1}^{n,r} - \phi_{i,j}^{n,r}}{\Delta y} \right)^2 \\
 & + \Delta y \sum_{j=1}^N \left(f_w(\phi_{1,j}^{n,r}) + f_w(\phi_{N,j}^{n,r}) \right) + \Delta x \sum_{i=1}^N \left(f_w(\phi_{i,1}^{n,r}) + f_w(\phi_{i,N}^{n,r}) \right).
 \end{aligned}
 \tag{32}$$

It then follows that in the scheme (25) the discrete free energy at every x -direction iteration, so that

$$\mathcal{F}_\Delta(\rho^{n,r}) - \mathcal{F}_\Delta(\rho^{n,r-1}) \leq 0.$$

Proof. Multiply by $\xi_{i,r}^{n,r}$ in (25a) and sum up the result over the indices i and j , so that

$$\sum_{i,j=1}^N \xi_{i,j}^{n,r} \left(\phi_{i,j}^{n,r} - \phi_{i,j}^{n,r-1} \right) = -\frac{\Delta t}{\Delta x} \sum_{i=1}^N \xi_{i,j}^{n,r} \left(F_{i+\frac{1}{2},j}^{n,r} - F_{i-\frac{1}{2},j}^{n,r} \right).$$

By substituting in the previous equation the expression of $\xi_{i,j}^{n,r}$ in (25e), it follows that

$$\begin{aligned}
 \sum_{i,j=1}^N \left(\phi_{i,j}^{n,r} - \phi_{i,j}^{n,r-1} \right) \frac{\epsilon^2}{2} \left[(\Delta \phi)_{i,j}^{n,r-1} + (\Delta \phi)_{i,j}^{n,*} \right] = & \frac{\Delta t}{\Delta x} \sum_{i=1}^N \xi_{i,j}^{n,r} \left(F_{i+\frac{1}{2},j}^{n,r} - F_{i-\frac{1}{2},j}^{n,r} \right) \\
 & + \sum_{i,j=1}^N \left(\phi_{i,j}^{n,r} - \phi_{i,j}^{n,r-1} \right) \left(H'_c(\phi_{i,j}^{n,r}) - H'_e(\phi_{i,j}^{n,r-1}) \right) \\
 & + \frac{1}{\Delta x} \sum_{i,j=1}^N \left(\phi_{i,j}^{n,r} - \phi_{i,j}^{n,r-1} \right) W_{i,j}^x(\phi_{i,j}^{n,r}, \phi_{i,j}^{n,r-1}) \\
 & + \frac{1}{\Delta y} \sum_{i,j=1}^N \left(\phi_{i,j}^{n,r} - \phi_{i,j}^{n,r-1} \right) W_{i,j}^y(\phi_{i,j}^{n,r}, \phi_{i,j}^{n,r-1}).
 \end{aligned}
 \tag{33}$$

Considering now the definition of the discrete free energy in (32), the decay between the x -direction iterations at r and $r - 1$ yields

$$\begin{aligned}
(34) \quad \frac{\mathcal{F}_\Delta(\phi^{n,r}) - \mathcal{F}_\Delta(\phi^{n,r-1})}{\Delta x \Delta y} &= \sum_{i,j=1}^N \left(H_c(\phi_{i,j}^{n,r}) - H_c(\phi_{i,j}^{n,r-1}) \right) - \sum_{i,j=1}^N \left(H_e(\phi_{i,j}^{n,r}) - H_e(\phi_{i,j}^{n,r-1}) \right) \\
&+ \sum_{i=1}^{N-1} \sum_{j=1}^N \frac{\epsilon^2}{2} \left(\frac{(\phi_{i+1,j}^{n,r} - \phi_{i,j}^{n,r})^2}{\Delta x^2} - \frac{(\phi_{i+1,j}^{n,r-1} - \phi_{i,j}^{n,r-1})^2}{\Delta x^2} \right) \\
&+ \sum_{i=1}^N \sum_{j=1}^{N-1} \frac{\epsilon^2}{2} \left(\frac{(\phi_{i,j+1}^{n,r} - \phi_{i,j}^{n,r})^2}{\Delta y^2} - \frac{(\phi_{i,j+1}^{n,r-1} - \phi_{i,j}^{n,r-1})^2}{\Delta y^2} \right) \\
&+ \frac{1}{\Delta x} \sum_{j=1}^N \left(f_w(\phi_{1,j}^{n,r}) - f_w(\phi_{1,j}^{n,r-1}) + f_w(\phi_{N,j}^{n,r}) - f_w(\phi_{N,j}^{n,r-1}) \right) \\
&+ \frac{1}{\Delta y} \sum_{i=1}^N \left(f_w(\phi_{i,1}^{n,r}) - f_w(\phi_{i,1}^{n,r-1}) + f_w(\phi_{i,N}^{n,r}) - f_w(\phi_{i,N}^{n,r-1}) \right).
\end{aligned}$$

The next step is to expand the sums with the discrete gradients at the interfaces, which correspond to the second and third line of the expression in (34). For this we follow the same strategy as with the 1D proof in (23): firstly, we apply summation by parts in the x direction (for the sum depending on Δx^2) and in the y direction (for the sum depending on Δy^2); secondly, the boundary conditions in (28) are taken into account; and thirdly, we apply the definition of the discrete Laplacians (25f) and (25g) bearing in mind that $\phi_{i,j+1}^{n,r} = \phi_{i,j+1}^{n,r-1}$ and $\phi_{i,j-1}^{n,r} = \phi_{i,j-1}^{n,r-1}$ when $j \neq r$.

Such expansion leads to

$$\begin{aligned}
&\sum_{i=1}^{N-1} \sum_{j=1}^N \frac{\epsilon^2}{2} \left(\frac{(\phi_{i+1,j}^{n,r} - \phi_{i,j}^{n,r})^2}{\Delta x^2} - \frac{(\phi_{i+1,j}^{n,r-1} - \phi_{i,j}^{n,r-1})^2}{\Delta x^2} \right) \\
&+ \sum_{i=1}^N \sum_{j=1}^{N-1} \frac{\epsilon^2}{2} \left(\frac{(\phi_{i,j+1}^{n,r} - \phi_{i,j}^{n,r})^2}{\Delta y^2} - \frac{(\phi_{i,j+1}^{n,r-1} - \phi_{i,j}^{n,r-1})^2}{\Delta y^2} \right) \\
&= \sum_{i=1}^{N-1} \sum_{j=1}^N \frac{\epsilon^2}{2} \left(\frac{\phi_{i+1,j}^{n,r} - \phi_{i,j}^{n,r}}{\Delta x} + \frac{\phi_{i+1,j}^{n,r-1} - \phi_{i,j}^{n,r-1}}{\Delta x} \right) \left(\frac{\phi_{i+1,j}^{n,r} - \phi_{i,j}^{n,r}}{\Delta x} - \frac{\phi_{i+1,j}^{n,r-1} - \phi_{i,j}^{n,r-1}}{\Delta x} \right) \\
&+ \sum_{i=1}^N \sum_{j=1}^{N-1} \frac{\epsilon^2}{2} \left(\frac{\phi_{i,j+1}^{n,r} - \phi_{i,j}^{n,r}}{\Delta y} + \frac{\phi_{i,j+1}^{n,r-1} - \phi_{i,j}^{n,r-1}}{\Delta y} \right) \left(\frac{\phi_{i,j+1}^{n,r} - \phi_{i,j}^{n,r}}{\Delta y} - \frac{\phi_{i,j+1}^{n,r-1} - \phi_{i,j}^{n,r-1}}{\Delta y} \right)
\end{aligned}$$

$$\begin{aligned}
&= - \sum_{i=2}^{N-1} \sum_{j=1}^N \frac{\epsilon^2}{2} \left(\phi_{i,j}^{n,r} - \phi_{i,j}^{n,r-1} \right) \left(\frac{\phi_{i+1,j}^{n,r} - 2\phi_{i,j}^{n,r} + \phi_{i-1,j}^{n,r}}{\Delta x^2} + \frac{\phi_{i+1,j}^{n,r-1} - 2\phi_{i,j}^{n,r-1} + \phi_{i-1,j}^{n,r-1}}{\Delta x^2} \right) \\
&\quad + \sum_{j=1}^N \frac{\epsilon^2}{2} \left(\phi_{N,j}^{n,r} - \phi_{N,j}^{n,r-1} \right) \left(\frac{\phi_{N,j}^{n,r} - \phi_{N-1,j}^{n,r}}{\Delta x^2} + \frac{\phi_{N,j}^{n,r-1} - \phi_{N-1,j}^{n,r-1}}{\Delta x^2} \right) \\
&\quad - \sum_{j=1}^N \frac{\epsilon^2}{2} \left(\phi_{1,j}^{n,r} - \phi_{1,j}^{n,r-1} \right) \left(\frac{\phi_{2,j}^{n,r} - \phi_{1,j}^{n,r}}{\Delta x^2} + \frac{\phi_{2,j}^{n,r-1} - \phi_{1,j}^{n,r-1}}{\Delta x^2} \right) \\
(35) \quad &- \sum_{i=1}^N \sum_{j=2}^{N-1} \frac{\epsilon^2}{2} \left(\phi_{i,j}^{n,r} - \phi_{i,j}^{n,r-1} \right) \left(\frac{\phi_{i,j+1}^{n,r} - 2\phi_{i,j}^{n,r} + \phi_{i,j-1}^{n,r}}{\Delta y^2} + \frac{\phi_{i,j+1}^{n,r-1} - 2\phi_{i,j}^{n,r-1} + \phi_{i,j-1}^{n,r-1}}{\Delta y^2} \right) \\
&\quad + \sum_{i=1}^N \frac{\epsilon^2}{2} \left(\phi_{i,N}^{n,r} - \phi_{i,N}^{n,r-1} \right) \left(\frac{\phi_{i,N}^{n,r} - \phi_{i,N-1}^{n,r}}{\Delta y^2} + \frac{\phi_{i,N}^{n,r-1} - \phi_{i,N-1}^{n,r-1}}{\Delta y^2} \right) \\
&\quad - \sum_{i=1}^N \frac{\epsilon^2}{2} \left(\phi_{i,1}^{n,r} - \phi_{i,1}^{n,r-1} \right) \left(\frac{\phi_{i,2}^{n,r} - \phi_{i,1}^{n,r}}{\Delta y^2} + \frac{\phi_{i,2}^{n,r-1} - \phi_{i,1}^{n,r-1}}{\Delta y^2} \right) \\
&= - \sum_{i,j=1}^N \frac{\epsilon^2}{2} \left(\phi_{i,j}^{n,r} - \phi_{i,j}^{n,r-1} \right) \left[(\Delta\phi)_{i,j}^{n,*} + (\Delta\phi)_{i,j}^{n,r-1} \right].
\end{aligned}$$

where $\phi_{i,j-1}^{n,r} = \phi_{i,j-1}^{n,r-1}$ and $\phi_{i,j+1}^{n,r} = \phi_{i,j+1}^{n,r-1}$ due to (25a). The resultant expression (35) matches with the left-hand side in (33). The next step is to substitute (33) in (34), but at the same time recall that $W_{i,j}^x = 0$ unless $i = 1, N$ due to (26), and $W_{i,j}^y = 0$ unless $j = 1, N$ due to (27). It follows that

$$\begin{aligned}
\frac{\mathcal{F}_\Delta(\phi^{n,r}) - \mathcal{F}_\Delta(\phi^{n,r-1})}{\Delta x \Delta y} &= \sum_{i,j=1}^N \left(H_c(\phi_{i,j}^{n,r}) - H_c(\phi_{i,j}^{n,r-1}) - H'_c(\phi_{i,j}^{n,r}) \left(\phi_{i,j}^{n,r} - \phi_{i,j}^{n,r-1} \right) \right) \\
&\quad - \sum_{i,j=1}^N \left(H_e(\phi_{i,j}^{n,r}) - H_e(\phi_{i,j}^{n,r-1}) - H'_e(\phi_{i,j}^{n,r-1}) \left(\phi_{i,j}^{n,r} - \phi_{i,j}^{n,r-1} \right) \right) \\
&\quad + \frac{1}{\Delta x} \sum_{j=1}^N \left[\left(f_w(\phi_{1,j}^{n,r}) - f_w(\phi_{1,j}^{n,r-1}) \right) - \left(\phi_{1,j}^{n,r} - \phi_{1,j}^{n,r-1} \right) W_{1,j}^x(\phi_{1,j}^{n,r}, \phi_{1,j}^{n,r-1}) \right] \\
&\quad + \frac{1}{\Delta x} \sum_{j=1}^N \left[\left(f_w(\phi_{N,j}^{n,r}) - f_w(\phi_{N,j}^{n,r-1}) \right) - \left(\phi_{N,j}^{n,r} - \phi_{N,j}^{n,r-1} \right) W_{N,j}^x(\phi_{N,j}^{n,r}, \phi_{N,j}^{n,r-1}) \right] \\
&\quad + \frac{1}{\Delta y} \sum_{i=1}^N \left[f_w(\phi_{i,1}^{n,r}) - f_w(\phi_{i,1}^{n,r-1}) - \left(\phi_{i,1}^{n,r} - \phi_{i,1}^{n,r-1} \right) W_{i,1}^y(\phi_{i,1}^{n,r}, \phi_{i,1}^{n,r-1}) \right] \\
&\quad + \frac{1}{\Delta y} \sum_{i=1}^N \left[\left(f_w(\phi_{i,N}^{n,r}) - f_w(\phi_{i,N}^{n,r-1}) \right) - \left(\phi_{i,N}^{n,r} - \phi_{i,N}^{n,r-1} \right) W_{i,N}^y(\phi_{i,N}^{n,r}, \phi_{i,N}^{n,r-1}) \right] \\
&\quad - \frac{\Delta t}{\Delta x} \sum_{i=1}^N \xi_{i,j}^{n,r} \left(F_{i+\frac{1}{2},j}^{n,r} - F_{i-\frac{1}{2},j}^{n,r} \right).
\end{aligned}$$

Following now the same reasoning as with the proof of the 1D case in Section 2, we get that the discrete free-energy dissipation in (32) is satisfied. \square

Lemma A.2. *Dissipation of the discrete free energy in each y -direction iteration. Let the discrete free energy of (2) for a particular c be defined as:*

$$\begin{aligned}
 \mathcal{F}_\Delta(\phi^{n,c}) = & \Delta x \Delta y \sum_{i,j=1}^n (H_c(\phi_{i,j}^{n,c}) - H_e(\phi_{i,j}^{n,c})) \\
 (36) \quad & + \Delta x \Delta y \sum_{i=1}^{N-1} \sum_{j=1}^N \frac{\epsilon^2}{2} \left(\frac{\phi_{i+1,j}^{n,c} - \phi_{i,j}^{n,c}}{\Delta x} \right)^2 + \Delta x \Delta y \sum_{i=1}^N \sum_{j=1}^{N-1} \frac{\epsilon^2}{2} \left(\frac{\phi_{i,j+1}^{n,c} - \phi_{i,j}^{n,c}}{\Delta y} \right)^2 \\
 & + \Delta y \sum_{j=1}^N (f_w(\phi_{1,j}^{n,c}) + f_w(\phi_{N,j}^{n,c})) + \Delta x \sum_{i=1}^N (f_w(\phi_{i,1}^{n,c}) + f_w(\phi_{i,N}^{n,c})).
 \end{aligned}$$

It then follows that for the scheme (29) the discrete free energy decays at every y -direction iteration, which in turn implies

$$\mathcal{F}_\Delta(\rho^{n,c}) - \mathcal{F}_\Delta(\rho^{n,c-1}) \leq 0.$$

Proof. The proof follows the same steps as in lemma A.1, and after some algebra, we obtain that the dissipation of discrete free energy (36) between the y -direction iterations at c and $c-1$ satisfies

$$\begin{aligned}
 \frac{\mathcal{F}_\Delta(\phi^{n,c}) - \mathcal{F}_\Delta(\phi^{n,c-1})}{\Delta x \Delta y} = & \sum_{i,j=1}^N \left(H_c(\phi_{i,j}^{n,c}) - H_c(\phi_{i,j}^{n,c-1}) - H'_c(\phi_{i,j}^{n,c}) (\phi_{i,j}^{n,c} - \phi_{i,j}^{n,c-1}) \right) \\
 & - \sum_{i,j=1}^N \left(H_e(\phi_{i,j}^{n,c}) - H_e(\phi_{i,j}^{n,c-1}) - H'_e(\phi_{i,j}^{n,c-1}) (\phi_{i,j}^{n,c} - \phi_{i,j}^{n,c-1}) \right) \\
 & + \frac{1}{\Delta x} \sum_{j=1}^N \left[(f_w(\phi_{1,j}^{n,c}) - f_w(\phi_{1,j}^{n,c-1})) - (\phi_{1,j}^{n,c} - \phi_{1,j}^{n,c-1}) W_{1,j}^x(\phi_{1,j}^{n,c}, \phi_{1,j}^{n,c-1}) \right] \\
 & + \frac{1}{\Delta x} \sum_{j=1}^N \left[(f_w(\phi_{N,j}^{n,c}) - f_w(\phi_{N,j}^{n,c-1})) - (\phi_{N,j}^{n,c} - \phi_{N,j}^{n,c-1}) W_{N,j}^x(\phi_{N,j}^{n,c}, \phi_{N,j}^{n,c-1}) \right] \\
 & + \frac{1}{\Delta y} \sum_{i=1}^N \left[f_w(\phi_{i,1}^{n,c}) - f_w(\phi_{i,1}^{n,c-1}) - (\phi_{i,1}^{n,c} - \phi_{i,1}^{n,c-1}) W_{i,1}^y(\phi_{i,1}^{n,c}, \phi_{i,1}^{n,c-1}) \right] \\
 & + \frac{1}{\Delta y} \sum_{i=1}^N \left[(f_w(\phi_{i,N}^{n,c}) - f_w(\phi_{i,N}^{n,c-1})) - (\phi_{i,N}^{n,c} - \phi_{i,N}^{n,c-1}) W_{i,N}^y(\phi_{i,N}^{n,c}, \phi_{i,N}^{n,c-1}) \right] \\
 & - \frac{\Delta t}{\Delta y} \sum_{i,j=1}^N \xi_{i,j}^{n,c} \left(F_{i+\frac{1}{2},j}^{n,c} - F_{i-\frac{1}{2},j}^{n,c} \right).
 \end{aligned}$$

Following once again the same reasoning as with the proof of the 1D case in Section 2, proves that the discrete free-energy dissipation in (36) is satisfied. \square

REFERENCES

- [1] H. ABELS AND M. WILKE, *Convergence to equilibrium for the Cahn–Hilliard equation with a logarithmic free energy*, Nonlinear Analysis: Theory, Methods & Applications, 67 (2007), pp. 3176–3193.
- [2] A. C. ARISTOTELOUS, O. KARAKASHIAN, AND S. M. WISE, *A mixed discontinuous Galerkin, convex splitting scheme for a modified Cahn–Hilliard equation and an efficient nonlinear multigrid solver*, Discrete & Continuous Dynamical Systems-B, 18 (2013), p. 2211.
- [3] B. AYMARD, U. VAES, M. PRADAS, AND S. KALLIADASIS, *A linear, second-order, energy stable, fully adaptive finite element method for phase-field modelling of wetting phenomena*, Journal of Computational Physics: X, 2 (2019), p. 100010.
- [4] R. BAILO, J. A. CARRILLO, AND J. HU, *Bound-Preserving Finite-Volume Schemes for Continuity Equations with Saturation*, work in preparation.

- [5] ———, *Fully Discrete Positivity-Preserving and Energy-Dissipating Schemes for Aggregation-Diffusion Equations with a Gradient Flow Structure*, Communications in Mathematical Sciences, 18 (2020), pp. 1259–1303.
- [6] R. BAILO, J. A. CARRILLO, H. MURAKAWA, AND M. SCHMIDTCHEN, *Convergence of a fully discrete and energy-dissipating finite-volume scheme for aggregation-diffusion equations*, arXiv: 2002.10821 (M3AS, to appear), (2020).
- [7] L. BAÑAS AND R. NÜRNBERG, *Adaptive finite element methods for cahn–hilliard equations*, Journal of computational and applied mathematics, 218 (2008), pp. 2–11.
- [8] J. W. BARRETT, J. F. BLOWEY, AND H. GARCKE, *Finite element approximation of the Cahn–Hilliard equation with degenerate mobility*, SIAM Journal on Numerical Analysis, 37 (1999), pp. 286–318.
- [9] ———, *On fully practical finite element approximations of degenerate Cahn–Hilliard systems*, ESAIM: Mathematical Modelling and Numerical Analysis, 35 (2001), pp. 713–748.
- [10] A. L. BERTOZZI, S. ESEDOGLU, AND A. GILLETTE, *Inpainting of binary images using the Cahn–Hilliard equation*, IEEE Transactions on image processing, 16 (2007), pp. 285–291.
- [11] M. BESSEMOULIN-CHATARD AND F. FILBET, *A finite volume scheme for nonlinear degenerate parabolic equations*, SIAM Journal on Scientific Computing, 34 (2012), pp. B559–B583.
- [12] F. BOYER, L. CHUPIN, AND P. FABRIE, *Numerical study of viscoelastic mixtures through a Cahn–Hilliard flow model*, European Journal of Mechanics - B/Fluids, 23 (2004), pp. 759 – 780.
- [13] M. BURGER, L. HE, AND C.-B. SCHÖNLIEB, *Cahn–Hilliard inpainting and a generalization for grayvalue images*, SIAM Journal on Imaging Sciences, 2 (2009), pp. 1129–1167.
- [14] L. A. CAFFARELLI AND N. E. MULER, *An l infinity bound for solutions of the Cahn–Hilliard equation*, ArMA, 133 (1995), pp. 129–144.
- [15] J. W. CAHN, *Critical point wetting*, The Journal of Chemical Physics, 66 (1977), pp. 3667–3672.
- [16] J. W. CAHN AND J. E. HILLIARD, *Free energy of a nonuniform system. i. interfacial free energy*, The Journal of Chemical Physics, 28 (1958), pp. 258–267.
- [17] J. A. CARRILLO, M. J. CASTRO, S. KALLIADASIS, AND S. P. PEREZ, *High-order well-balanced finite-volume schemes for hydrodynamic equations with nonlocal free energy*, SIAM Journal on Scientific Computing, 43 (2021), pp. A828–A858.
- [18] J. A. CARRILLO, A. CHERTOCK, AND Y. HUANG, *A finite-volume method for nonlinear nonlocal equations with a gradient flow structure*, Communications in Computational Physics, 17 (2015), pp. 233–258.
- [19] J. A. CARRILLO, S. KALLIADASIS, F. LIANG, AND S. P. PEREZ, *Enhancement of damaged-image prediction through Cahn–Hilliard image inpainting*, arXiv preprint arXiv:2007.10753, (2020).
- [20] J. A. CARRILLO, S. KALLIADASIS, S. P. PEREZ, AND C.-W. SHU, *Well-balanced finite-volume schemes for hydrodynamic equations with general free energy*, Multiscale Modeling & Simulation, 18 (2020), pp. 502–541.
- [21] M. CATES, J.-C. DESPLAT, P. STANSELL, A. WAGNER, K. STRATFORD, R. ADHIKARI, AND I. PAGONABARRAGA, *Physical and computational scaling issues in lattice boltzmann simulations of binary fluid mixtures*, Philosophical Transactions of the Royal Society A: Mathematical, Physical and Engineering Sciences, 363 (2005), pp. 1917–1935.
- [22] C. CHEN AND X. YANG, *Fast, provably unconditionally energy stable, and second-order accurate algorithms for the anisotropic Cahn–Hilliard model*, Computer Methods in Applied Mechanics and Engineering, 351 (2019), pp. 35–59.
- [23] W. CHEN, C. WANG, X. WANG, AND S. M. WISE, *Positivity-preserving, energy stable numerical schemes for the Cahn–Hilliard equation with logarithmic potential*, Journal of Computational Physics: X, 3 (2019), p. 100031.
- [24] A. CHRISTLIEB, J. JONES, K. PROMISLOW, B. WETTON, AND M. WILLOUGHBY, *High accuracy solutions to energy gradient flows from material science models*, Journal of Computational Physics, 257 (2014), pp. 193–215.
- [25] N. CONDETTE, C. MELCHER, AND E. SÜLI, *Spectral approximation of pattern-forming nonlinear evolution equations with double-well potentials of quadratic growth*, Mathematics of computation, 80 (2011), pp. 205–223.
- [26] M. COPETTI AND C. M. ELLIOTT, *Numerical analysis of the Cahn–Hilliard equation with a logarithmic free energy*, Numerische Mathematik, 63 (1992), pp. 39–65.
- [27] L. CUETO-FELGUEROSO AND J. PERAIRE, *A time-adaptive finite volume method for the Cahn–Hilliard and kuramoto–sivashinsky equations*, Journal of Computational Physics, 227 (2008), pp. 9985–10017.
- [28] A. E. DIEGEL, C. WANG, AND S. M. WISE, *Stability and convergence of a second-order mixed finite element method for the Cahn–Hilliard equation*, IMA Journal of Numerical Analysis, 36 (2016), pp. 1867–1897.
- [29] M. DOI, *Soft matter physics*, Oxford University Press, 2013.
- [30] C. M. ELLIOTT AND H. GARCKE, *On the Cahn–Hilliard equation with degenerate mobility*, SIAM Journal on Mathematical Analysis, 27 (1996), pp. 404–423.
- [31] D. J. EYRE, *Unconditionally gradient stable time marching the Cahn–Hilliard equation*, MRS Online Proceedings Library Archive, 529 (1998).
- [32] F. FRANK, A. RUPP, AND D. KUZMIN, *Bound-preserving flux limiting schemes for dg discretizations of conservation laws with applications to the Cahn–Hilliard equation*, Computer Methods in Applied Mechanics and Engineering, 359 (2020), p. 112665.
- [33] D. FURIHATA, *A stable and conservative finite difference scheme for the Cahn–Hilliard equation*, Numerische Mathematik, 87 (2001), pp. 675–699.
- [34] H. GARCKE, K. F. LAM, R. NÜRNBERG, AND E. SITKA, *A multiphase cahn–hilliard–darcy model for tumour growth with necrosis*, Mathematical Models and Methods in Applied Sciences, 28 (2018), pp. 525–577.

- [35] H. GÓMEZ, V. M. CALO, Y. BAZILEVS, AND T. J. HUGHES, *Isogeometric analysis of the Cahn–Hilliard phase-field model*, Computer methods in applied mechanics and engineering, 197 (2008), pp. 4333–4352.
- [36] J. GUO, C. WANG, S. M. WISE, AND X. YUE, *An h^2 convergence of a second-order convex-splitting, finite difference scheme for the three-dimensional Cahn–Hilliard equation*, Communications in Mathematical Sciences, 14 (2016), pp. 489–515.
- [37] K. A. HAWICK AND D. P. PLAYNE, *Modelling and visualizing the Cahn–Hilliard-cook equation.*, in MSV, 2008, pp. 149–155.
- [38] Y. HE, Y. LIU, AND T. TANG, *On large time-stepping methods for the Cahn–Hilliard equation*, Applied Numerical Mathematics, 57 (2007), pp. 616–628.
- [39] M. HINTERMÜLLER, M. HINZE, AND M. H. TBER, *An adaptive finite-element moreau–yosida-based solver for a non-smooth Cahn–Hilliard problem*, Optimization Methods and Software, 26 (2011), pp. 777–811.
- [40] D. KIM AND W. LU, *Three-dimensional model of electrostatically induced pattern formation in thin polymer films*, Physical Review B, 73 (2006), p. 035206.
- [41] J. KIM, S. LEE, Y. CHOI, S.-M. LEE, AND D. JEONG, *Basic principles and practical applications of the Cahn–Hilliard equation*, Mathematical Problems in Engineering, 2016 (2016).
- [42] D. LEE, J.-Y. HUH, D. JEONG, J. SHIN, A. YUN, AND J. KIM, *Physical, mathematical, and numerical derivations of the Cahn–Hilliard equation*, Computational Materials Science, 81 (2014), pp. 216–225.
- [43] H. G. LEE AND J. KIM, *Accurate contact angle boundary conditions for the Cahn–Hilliard equations*, Computers & fluids, 44 (2011), pp. 178–186.
- [44] A. MIRANVILLE AND S. ZELIK, *Robust exponential attractors for Cahn–Hilliard type equations with singular potentials*, Mathematical methods in the applied sciences, 27 (2004), pp. 545–582.
- [45] S. P. PEREZ, *Code to reproduce the one- and two-dimensional Cahn–Hilliard simulations*. https://github.com/sergioperez/Cahn_Hilliard_Finite_Volume, Mar 2021.
- [46] S. P. PEREZ, *Films of the two-dimensional simulations*. https://figshare.com/projects/Unconditional_bound-preserving_and_energy-dissipating_finite-volume_schemes_for_the_Cahn-Hilliard_equation/101126, Mar 2021.
- [47] M. QUERALT-MARTÍN, M. PRADAS, R. RODRÍGUEZ-TRUJILLO, M. ARUNDELL, E. C. POIRÉ, AND A. HERNÁNDEZ-MACHADO, *Pinning and avalanches in hydrophobic microchannels*, Physical review letters, 106 (2011), p. 194501.
- [48] A. RUSSO, S. P. PEREZ, M. A. DURÁN-OLIVENCIA, P. YATSYSHIN, J. A. CARRILLO, AND S. KALLIADASIS, *A finite-volume method for fluctuating dynamical density functional theory*, Journal of Computational Physics, (2020), p. 109796.
- [49] P. SEPPACHER, *Moving contact lines in the Cahn–Hilliard theory*, International journal of engineering science, 34 (1996), pp. 977–992.
- [50] J. SHEN, J. XU, AND J. YANG, *The scalar auxiliary variable (sav) approach for gradient flows*, Journal of Computational Physics, 353 (2018), pp. 407–416.
- [51] ———, *A new class of efficient and robust energy stable schemes for gradient flows*, SIAM Review, 61 (2019), pp. 474–506.
- [52] J. SHEN AND X. YANG, *Numerical approximations of Allen–Cahn and Cahn–Hilliard equations*, Discrete & Continuous Dynamical Systems-A, 28 (2010), p. 1669.
- [53] D. N. SIBLEY, A. NOLD, AND S. KALLIADASIS, *Unifying binary fluid diffuse-interface models in the sharp-interface limit*, Journal of fluid mechanics, 736 (2013), p. 5.
- [54] D. N. SIBLEY, A. NOLD, N. SAVVA, AND S. KALLIADASIS, *The contact line behaviour of solid–liquid–gas diffuse-interface models*, Physics of Fluids, 25 (2013), p. 092111.
- [55] ———, *On the moving contact line singularity: Asymptotics of a diffuse-interface model*, The European Physical Journal E, 36 (2013), p. 26.
- [56] A. F. STALDER, G. KULIK, D. SAGE, L. BARBIERI, AND P. HOFFMANN, *A snake-based approach to accurate determination of both contact points and contact angles*, Colloids and surfaces A: physicochemical and engineering aspects, 286 (2006), pp. 92–103.
- [57] G. TIERRA AND F. GUILLÉN-GONZÁLEZ, *Numerical methods for solving the Cahn–Hilliard equation and its applicability to related energy-based models*, Archives of Computational Methods in Engineering, 22 (2015), pp. 269–289.
- [58] X. WU, G. VAN ZWIETEN, AND K. VAN DER ZEE, *Stabilized second-order convex splitting schemes for Cahn–Hilliard models with application to diffuse-interface tumor-growth models*, International journal for numerical methods in biomedical engineering, 30 (2014), pp. 180–203.
- [59] C. WYLOCK, M. PRADAS, B. HAUT, P. COLINET, AND S. KALLIADASIS, *Disorder-induced hysteresis and nonlocality of contact line motion in chemically heterogeneous microchannels*, Physics of fluids, 24 (2012), p. 032108.
- [60] Y. XIA, Y. XU, AND C.-W. SHU, *Local discontinuous Galerkin methods for the Cahn–Hilliard type equations*, Journal of Computational Physics, 227 (2007), pp. 472–491.
- [61] J. XU, Y. LI, S. WU, AND A. BOUSQUET, *On the stability and accuracy of partially and fully implicit schemes for phase field modeling*, Computer Methods in Applied Mechanics and Engineering, 345 (2019), pp. 826–853.
- [62] J. ZHANG, C. CHEN, AND X. YANG, *Efficient and energy stable method for the Cahn–Hilliard phase-field model for diblock copolymers*, Applied Numerical Mathematics, 151 (2020), pp. 263–281.

- [63] S. ZHOU AND M. Y. WANG, *Multimaterial structural topology optimization with a generalized Cahn–Hilliard model of multiphase transition*, Structural and Multidisciplinary Optimization, 33 (2007), p. 89.